FINITE ELEMENTS FOR FREE EDGE DELAMINATIONS
AND DELAMINATED ANISOTROPIC BEAMS

BY
MARCO ANTONIO SANTOS PINHEIRO

A DISSERTATION PRESENTED TO THE GRADUATE SCHOOL
OF THE UNIVERSITY OF FLORIDA IN PARTIAL FULFILLMENT
OF THE REQUIREMENTS FOR THE DEGREE OF
DOCTOR OF PHILOSOPHY

UNIVERSITY OF FLORIDA

1991

In memory of my father-in-law

Fernando Pinto

still and forever a beacon to my family

ACKNOWLEDGMENTS

I would like to express my sincere gratitude to my advisor Dr. Bhavani V. Sankar for his continuous support, encouragement and constructive criticism during all my doctoral studies. His competence and understanding of his students always impressed me and are examples to be followed in my future life. Gratitude is extended to Professors U.H. Kurzweg, L.E. Malvern, M. Rao and C.T. Sun, members of my doctoral supervisory committee, for their assistance during my research. My appreciation goes to Dr. C.E. Taylor for his participation in the initial part of my work.

Special thanks are owed to the Brazilian Army for giving me the opportunity to come to the United States of America to pursue doctoral studies.

I would like to thank my friends at the Department of Aerospace Engineering, Mechanics and Engineering Science, whose friendship have been motivation for the completion of this work.

Finally, I am grateful to my wife, Fernanda, my daughter Simone, my son Luis Marco, my parents Jose and Nely, and my mother-in-law Geny. They have been always a source of encouragement, support and love.

TABLE OF CONTENTS

LIST OF TABLES

LIST OF FIGURES

Abstract of Dissertation Presented to the Graduate School
of the University of Florida in Partial Fulfillment of the
Requirements for the Degree of Doctor of Philosophy

FINITE ELEMENTS FOR FREE EDGE DELAMINATIONS
AND DELAMINATED ANISOTROPIC BEAMS

By

Marco Antonio Santos Pinheiro

December, 1991

Chairman: Dr. Bhavani V. Sankar
Major Department: Aerospace Engineering, Mechanics, and
Engineering Science

The major objective of this study is to develop a
technique to analyze delaminations in composite beams by using
the finite element method.

A method is proposed to obtain the strain energy release
rate and the stresses ahead of the crack for the specific case
of free edge delaminations. A shear deformable beam finite
element with nodes offset to either top or bottom side has
been developed. The thermal effects originating from the
curing process are included in the formulation of the problem.

Three different expressions to calculate the strain
energy release rate are derived, one in terms of the force and
moment resultants in the elements surrounding the crack-tip,
and the two others in terms of the forces transmitted by a
rigid element placed at the tip of the crack. The stresses
ahead of the crack are obtained by using discrete spring

elements in the uncracked portion of the beam. The results calculated are in good agreement with results obtained from other studies of the same problem. The advantage of using the present method is that it requires less computational effort, and is capable of modeling any type of geometry, loading, and boundary conditions.

An efficient beam finite element has been developed based on a generalized beam theory for anisotropic beams, in which the equilibrium equations are assumed to be satisfied in an average sense over the width of the beam. This introduces a new set of force and moment resultants for the beam. The displacements in the beam are expressed in terms of three deflections, three rotations and one warping term. The effectiveness of the method is illustrated by solving problems where the beam theory solutions are known. The strain energy release rate is determined for the cases of delaminated cantilever beam under torsion and simply supported delaminated beam under transverse loading. Studies are performed to understand the influence of the position of the delamination on the strain energy release rate.

CHAPTER 1

INTRODUCTION

1.1 Motivation and Objectives

Structural materials can bear defects proceeding from the fabrication processes or accumulate damage during their service life. Frequently, such defects and damage are not visually observable and have to be detected by using non-destructive evaluation techniques (NDE).

In a variety of applications, such as aerospace and aircraft structures, offshore platforms, bridges and tall buildings, the replacement of the imperfect parts is not a cost-effective solution for the problem. The costs involved in keeping the equipment out of order, the difficulty of access, and other reasons suggest that there is a need for research and development of methods to predict the occurrence and extent of the damages.

Composite materials and structures, for example, are highly susceptible to damage from low-energy impacts. Incidents such as tool-drops, improper handling or hailstorms (aircraft structures) can cause internal damage and significant reduction in compressive strength of the material. Under subsequent transverse loadings, the damage will grow

1

causing a redistribution of the stresses in the plies of a laminate and consequently reduction in the material stiffness and fatigue life. However, depending on the subsequent loading conditions and the damage characteristics, the structure often can still be used despite the existence of damage.

Failure in a composite material often initiates in the form of a matrix crack or a delamination. The former refers to intralaminar failure or transverse crack, while the latter refers to interlaminar failure. Both types of failures are illustrated in Fig. 1.1.

Delamination, or separation of the layers, is a mode of failure unique to laminated materials, and it is the predominant failure mode in continuous fiber composites. Based on the location and direction of the growth, we can discern two types of delamination: the free edge delamination and the transverse delamination. In the edge delamination the growth initiates at the load-free edges of the laminate and propagates normal to the load direction. Under transverse delamination, also known as crack tip or local delamination, the growth starts from a matrix crack and propagates normal to the transverse crack from which it originates. The Fig. 1.2 shows both types of delamination. Since delamination is a very commonly observed failure mode in composite materials, its study is of great importance in the field of failure prediction for composite structures.
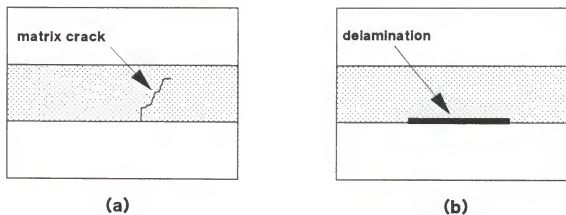
Figure 1.1 Failures in composite materials
(a) Matrix crack (b) Delamination
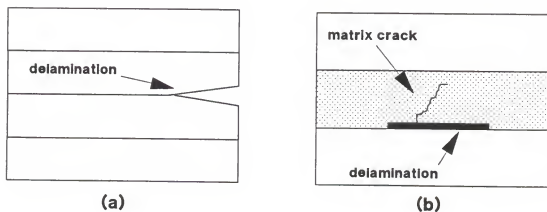
Figure 1.2 Types of delamination
(a) Free edge (b) Transverse delamination

1.2 Literature Survey

In the past few years, several researchers have studied delamination occurrence and growth. Usually they predict delamination growth from the strain energy release rate (G), and try to develop analytical and numerical methods capable of modeling this phenomenon. A brief description of some of these studies is important for accurate comprehension of the present work.

Chan and Ochoa (1987) developed a two-dimensional finite element model to calculate interlaminar stresses and strain energy release rate in composites subjected to uniaxial tension, bending and torsion. The element is an isoparametric element with eight nodes and three degrees of freedom per node. The basic idea in their work is to represent the effect of longitudinal or twisting curvature as a "load effect." The study concentrates on establishing relationships of G_I, G_{II} and G_{III} as functions of crack length and stacking sequence.

Pagano (1974) studied the case of fibrous composite laminates under a uniform axial extension and developed an approximate method to define the distribution of the interlaminar normal stress along the central plane of a symmetric laminate. A simple expression for the interlaminar normal stress was derived and the results obtained by using this expression were compared with those obtained by using a finite difference approximation of the elasticity equations. The two methods agreed well, and both results show that

significant stresses exist only in narrow regions next to the free edges. The length of this region is approximately equal to the laminate thickness.

Whitney (1986) proposed an approximation to the interlaminar normal stress distribution ahead of the crack and the influence of specimen geometry on Mode I strain energy release rate for edge delamination specimens. The specimens were subjected to tension and compression loadings and were of the classes $[0_3/90_3]_s$ or $[\theta/-\theta_2/\theta/90_2]_s$. Whitney used a higher order plate theory, which considers transverse shear deformation and thickness-stretching. The effect of thermal residual stresses due to lamination fabrication was considered in the formulation of the problem. The numerical results suggested significant influence of the residual thermal stresses on both the stress distribution ahead of the crack and the Mode I strain energy release rate. In general, the thermal residual stresses increase the stresses at crack tip and the Mode I strain energy release rate for specimens under tension, and has the inverse effect for specimens under compression. Again the results confirmed that the effect of normal stress ahead of the crack dissipates within a distance of approximately twice the thickness from the crack front.

Armanios and Badir (1989) used a shear deformation theory to calculate the interlaminar stresses and energy release rate associated with both Mode I and mixed-mode edge delaminations. The formulation used by Armanio and Badir does not consider

the thickness strain effect. The analysis includes the effects caused by the residual thermal stresses and moisture stresses. The classes of laminates considered are the same ones used by Whitney (1986). Results suggest that the residual thermal stresses tend to increase the interlaminar stresses and total energy release rate for both modes, while the moisture content tends to alleviate the thermal effects. The value of moisture content necessary to alleviate totally the interlaminar stresses and the strain energy release rate ranged between 0.70% and 0.80% in the examples considered, and it was found that this value has a weak dependency on both the stacking sequence and the mode considered.

Usman and Gandhi (1989) studied the effect of moisture and temperature on the vibrational characteristics of composite materials. The nonlinear vibration of moderately-thick laminated composite plates under hygro-thermal conditions are considered by incorporating the effects of transverse shear and rotary inertia. The hygro-thermal changes along the thickness of the composite were explicitly incorporated in the form of the deformation field. The response of the composite under hygro-thermal environments was modeled by creating one model formed by two parts, one anisotropic solid (composite) and one ideal fluid (moisture). The equations presented in this work are significantly different from the corresponding equations in classical laminated composite plate theory.

Hu et al.(1989) developed a novel beam element to study the crack propagation in beam types of specimens. Finite elements are used to model the specimens, and the beam element has its nodes offset to one side, either bottom or top side. This approach allows modeling crack propagation without renumbering the nodes as the crack propagates, and is convenient in modeling the partial contact and slip at a delamination interface. The bottom and top un-delaminated portions of the beam were connected either by foundation springs or rigid elements. For some specimens the strain energy release rate was computed by using a zero-volume path integral and a crack closure method, and the results were found to be in good agreement. In the present study the beam theory is extended to analyze delaminated composite beams.

Sankar (1991 b) developed a beam theory for laminated composite beams derived from the shear deformable plate theory. The equilibrium equations are assumed to be satisfied in an average sense over the width of the beam, which introduces a new set of force and moment resultants for the beam. The displacements in the beam are expressed in terms of three deflections, three rotations, and one warping term. The closed solutions for the cases of a cantilever beam subjected to end loads and a specially orthotropic laminate beam under torsional loading are presented. The solution considers the shear deformation and the edge effect. The results in terms of angle of twist agree well with available solutions.

1.3 Scope and Outline of this Work

Numerical and analytical methods have been used to express the complex stress state near free edges and to calculate the energy release rate during crack propagation. Among several numerical methods, the finite element method was selected to be used in the present work. Although requiring intensive computational effort, this method is very popular and provides accurate solutions. Also, this method is very convenient in modeling structural elements of variable cross section.

In the present work, the typical element used to model the structure is the beam element. This element not only is very common in mechanical structures but also is the most appropriate to model some standard test specimens.

The scope of this work can be described as to develop a method to analyze delaminations in anisotropic composite beams, using the finite element method to model the problem and selecting the strain energy release rate as a delamination parameter. The loading is considered independent of time.

This dissertation consists of five chapters. Chapter 2 is focused on free edge delamination. A method is proposed for modeling this type of delamination using offset beam finite elements. The effect of temperature variation during the curing process (residual stresses) is considered in the problem. Chapters 3 and 4 are devoted to presenting a new and

efficient method to analyze composite laminated beams, using a more complete and accurate beam finite element. The capability of this new finite element in modeling the problem was verified by solving the problem of a cantilever beam subjected to different end loading conditions, including torsion. Applications to delaminated beams under torsion loading and the simulation of a quasi-static impact test on a delaminated beam are also presented in these chapters. Finally, chapter 5 summarizes the principal conclusions of the present study, and presents suggestions for future studies in this field.

CHAPTER 2

AN OFFSET BEAM FINITE ELEMENT FOR MODELING
FREE EDGE DELAMINATIONS IN COMPOSITES

2.1 Introduction

The separation of plies or delamination is a predominant failure mode in laminated composite structures. It occurs when interlaminar stresses exceed the interlaminar strength of the material, or as a result of the fabrication process, environmental degradation and improper handling of the material. Common examples of such failure regions during the normal use of composite structures are those near cut-outs, holes and free edges. In these regions, the abrupt changes in the geometry or material properties tend to intensify the stresses when the laminate is subjected to some external loads.

Specifically, the occurrence of delamination in free edges has been receiving increasing attention of many investigators, in their efforts to understand and to prevent delaminations in composite structural designs. The reason is the presence of high interlaminar stresses, the "peeling" stress, in the neighborhood of a free boundary. The "free edge problem" usually is modeled by a plate subjected to a uniform axial strain (e_0), as shown in Fig. 2.1.

10
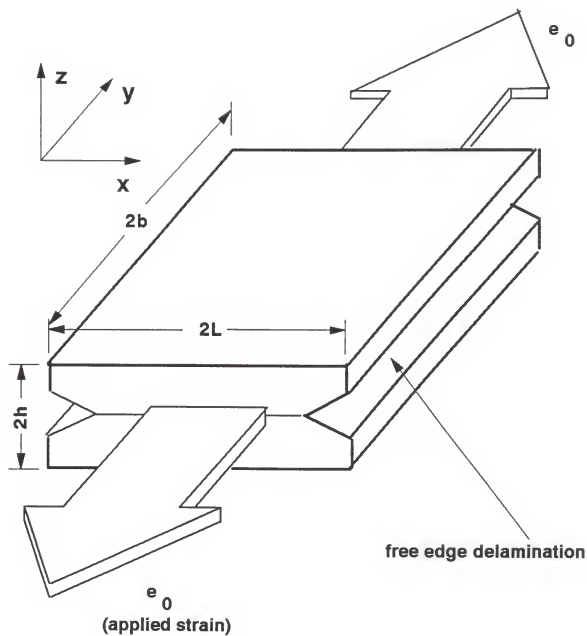
Figure 2.1 Free edge delamination

During the usual fabrication process, the composite material is subjected to temperatures of several hundred degrees Fahrenheit, and then it is cooled down to the room temperature. The composite is assumed to be stress-free at the curing temperature. The change in temperature causes unavoidable stresses to the composite material layers when cooled to room temperature. Usually these stresses are called residual stresses or thermal stresses, and they are considered in the formulation of the present problem.

A simple procedure is developed in this study to obtain an approximate solution for the peel stresses ahead of the crack tip and to calculate the strain energy release rate, for the case of free edge delaminations including thermal effects. The problem depicted in Figure 2.1 is modeled using a shear deformable beam finite element with offset nodes (Sankar, 1989). The three-dimensional problem is modeled as a plane problem in the x-z plane assuming that the stresses and strains do not vary along the y-direction. This will be true for most of the length of the plate in the y-direction. The delamination plane divides the beam into two parts, the top sublaminate and the bottom sublaminate (Figure 2.2), with nodes offset to the bottom and top, respectively. The delamination plane is assumed to be the weakest one, therefore the crack propagates along this plane, without crack branchings.
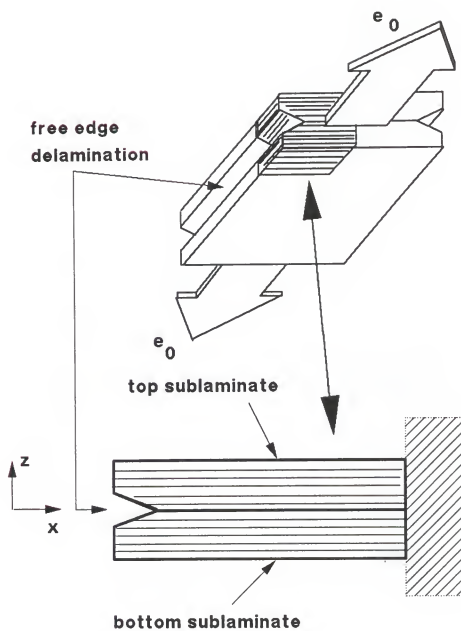
Figure 2.2 Sublaminates

When calculating the energy release rate, the uncracked region of the beam is connected by common nodes, except the tip of the crack, where a rigid element is used to connect the top and bottom nodes (Fig. 2.3). This rigid element not only ensures the continuity of displacements and rotations at that section, but also brings in its formulation the generalized forces that are transmitted between the sublaminates. These forces are used in the calculation of the energy release rate. In evaluating the peel stresses ahead of the crack, the uncracked region of the beam is connected by spring elements (Fig. 2.4), stiffness of which has to be judiciously selected.

The strain energy release rate has been successfully adopted by researchers in characterizing delamination. In this study its value is obtained from three different methods (Sankar and Pinheiro, 1990). The first one uses in its formulation the forces transmitted by the crack-tip rigid element. In the second method, the result is obtained by using a method similar to the crack-closure method used in two-dimensional fracture problems. Finally, composites are very brittle materials, so that, the plastic zone in the vicinity of the crack tip is negligible, and hence the linear elastic fracture mechanics can be applied in which case the J-integral is equivalent to the energy release rate. Therefore, the third method consists in obtaining the J-integral from the beam model. The force and moment resultants in the region surrounding the crack-tip are used in this calculation.
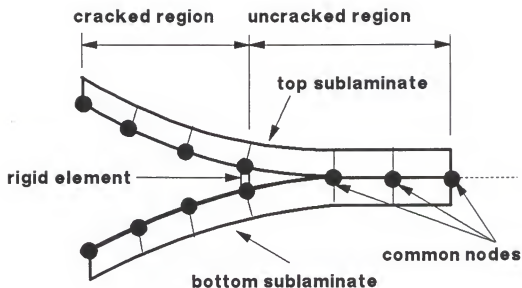
Figure 2.3 Finite element model for strain energy
release rate
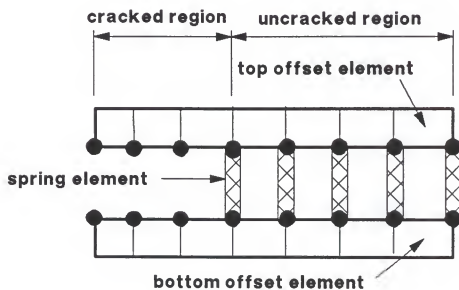
Figure 2.4 Finite element model for peel stresses

The results from the three different methods are compared and found to be in good agreement.

2.2 Laminated Beam

In this section a homogeneous orthotropic laminate subjected to a uniform initial strain $\epsilon_{yy} = e_0$ applied over a length 2L is analyzed. The thickness of the laminate is 2h and the width is 2b. The thickness 2h is much smaller than 2L and 2L much smaller than 2b (Fig. 2.1). Due to symmetry conditions, just one half of the laminate is considered here.

The problem is divided into two different phases. In the first phase no initial strain is applied to the specimen, which is subjected only to thermal stresses due to the curing process. In the second phase the cured specimen containing the edge delamination is subjected to the axial strain $\epsilon_{yy} = e_0$ in addition to the residual stresses.

The equations derived in the next sections refer to a laminated beam situated above the delamination plane. The expressions for the laminated beam situated below the delamination plane differ only in the integration limits (-h to 0, instead of 0 to h).

2.3 Fabrication Process

During the composite fabrication process there are heating and cooling phases. In the cooling phase, the temperature drops from the stress-free temperature to the room

temperature. In this case, each layer influences the expansion or contraction of the other because of the difference in their coefficient of thermal expansion. A similar situation exists when the composite absorbs moisture during service. As a result of the temperature variation, each layer has residual stresses after the laminate fabrication.

The effects of the residual stresses on the laminate as a whole are calculated and expressed in terms of thermal forces and moments. In the next phase, these thermal forces and moments are added to the external forces and moments.

During the cooling process the in-plane and transverse displacements are assumed to be of the form:

$$u(x,z) = u_0(x) + z\psi_x(x)$$
$$v(y,z) = v_0(y) + z\psi_y(y) \quad (2.1)$$
$$w(x,z) = w_0(x)$$

where u_0 and v_0 are the axial displacements of points on the x-y plane in the x and y directions respectively, and Ψ_x and Ψ_y are the rotations about the y and x axes respectively. It is assumed that the modification in the thickness of the laminate is negligible when compared with the modifications in the other two dimensions. Therefore, w is assumed to be constant through the thickness of the laminate (no thickness strain).

From Equations 2.1 the strains for the cooling process are derived as

$$
\begin{aligned}
\varepsilon_{xx} &= u_{0,x} + z\psi_{x,x} = \varepsilon_x^0 + z\kappa_x \\
\varepsilon_{yy} &= v_{0,y} + z\psi_{y,y} = \varepsilon_y^0 + z\kappa_y \\
\gamma_{zx} &= \psi_x + w_{,x}
\end{aligned} \tag{2.2}
$$

A state of plane stress normal to the z direction is assumed during the curing process. Therefore, the thermal stresses developed within the kth layer (Agarwal and Broutman, 1980) are

$$
\begin{pmatrix} \sigma_{xx} \\ \sigma_{yy} \\ \tau_{xy} \end{pmatrix}_k =
\begin{pmatrix} \overline{Q}_{11} \overline{Q}_{12} \overline{Q}_{16} \\ \overline{Q}_{12} \overline{Q}_{22} \overline{Q}_{26} \\ \overline{Q}_{16} \overline{Q}_{26} \overline{Q}_{66} \end{pmatrix}
\begin{pmatrix} \varepsilon_{xx} - \zeta_x \\ \varepsilon_{yy} - \zeta_y \\ -\zeta_{xy} \end{pmatrix} \tag{2.3}
$$

where Q_{ij} are the stiffness coefficients and can be found in Whitney (1987), and

$$
\begin{aligned}
\zeta_x &= \alpha_x \Delta T \\
\zeta_y &= \alpha_y \Delta T \\
\zeta_{xy} &= \alpha_{xy} \Delta T
\end{aligned} \tag{2.4}
$$

In the above equations α is the thermal expansion coefficient and ΔT is the change in temperature.

By definition, the force (N) and moment (M) acting on the top laminate are

$$
\begin{aligned}
(N_x, M_x) &= \int_0^h \sigma_x [1, z] \, dz \\
(N_y, M_y) &= \int_0^h \sigma_y [1, z] \, dz
\end{aligned} \tag{2.5}
$$

In the present case, there are no net resultants acting on the laminate. Therefore, considering the definition of force and moment resultants, we have for the whole laminate

$$\begin{pmatrix} N_x \\ N_y \end{pmatrix} = \begin{pmatrix} 0 \\ 0 \end{pmatrix} = \sum_{k=1}^{n} \int_{h_{k-1}}^{h_k} \begin{pmatrix} \sigma_x \\ \sigma_y \end{pmatrix}_k dz \qquad (2.6)$$

and

$$\begin{pmatrix} M_x \\ M_y \end{pmatrix} = \begin{pmatrix} 0 \\ 0 \end{pmatrix} = \sum_{k=1}^{n} \int_{h_{k-1}}^{h_k} \begin{pmatrix} \sigma_x \\ \sigma_y \end{pmatrix}_k z \, dz \qquad (2.7)$$

where n is the total number of layers on the top sublaminate and $(h_k - h_{k-1})$ is equal to the thickness of the kth layer (Fig. 2.5).
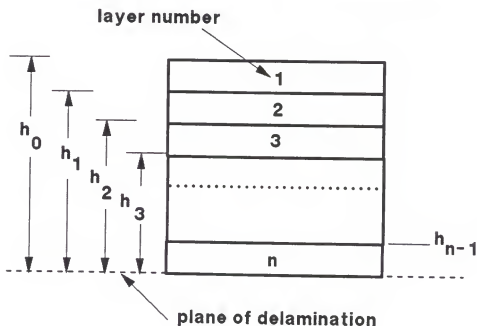
Figure 2.5 Values of h for top sublaminate

The stiffness coefficients of the top sublaminate are defined as

$$[a_{ij}, b_{ij}, d_{ij}] = \int_0^h \overline{Q}_{ij} [1, z, z^2] \; dz \qquad (2.8)$$

$$i, j = 1, 2, \ldots, 6$$

In the above equation, a shear correction factor equal to 5/6 (Whitney, 1987) is introduced in the calculation of the terms a_{ii}, b_{ii} and d_{ii}, wherever the index i is greater then 3.

Substituting Eq. 2.3 in Eq. 2.6 and 2.7, and using the definition of the stiffness coefficients in Eq. 2.8, we obtain the following expressions for the force and moment resultants

$$\begin{pmatrix} N_x \\ M_x \end{pmatrix} = \begin{pmatrix} 0 \\ 0 \end{pmatrix} - \begin{pmatrix} a_{11} & b_{11} \\ b_{11} & d_{11} \end{pmatrix} \begin{pmatrix} e_x^0 \\ \kappa_x \end{pmatrix} + \begin{pmatrix} a_{12} & b_{12} \\ b_{12} & d_{12} \end{pmatrix} \begin{pmatrix} e_x^0 \\ \kappa_x \end{pmatrix} - \begin{pmatrix} N_x^T \\ M_x^T \end{pmatrix} \qquad (2.9)$$

$$\begin{pmatrix} N_y \\ M_y \end{pmatrix} = \begin{pmatrix} 0 \\ 0 \end{pmatrix} - \begin{pmatrix} a_{12} & b_{12} \\ b_{12} & d_{12} \end{pmatrix} \begin{pmatrix} e_x^0 \\ \kappa_x \end{pmatrix} + \begin{pmatrix} a_{22} & b_{22} \\ b_{22} & d_{22} \end{pmatrix} \begin{pmatrix} e_y^0 \\ \kappa_y \end{pmatrix} - \begin{pmatrix} N_y^T \\ M_y^T \end{pmatrix} \qquad (2.10)$$

where N^T_x and M^T_x are the thermal force and moment in the x direction and so are N^T_y and M^T_y in the y direction.

The thermal forces and moments are defined as

$$[N_x^T, M_x^T] = \int_0^h (\overline{Q}_{11}\zeta_x + \overline{Q}_{12}\zeta_y + \overline{Q}_{16}\zeta_{xy}) \, [1, z] \, dz \qquad (2.11)$$

$$[N_y^T, M_y^T] = \int_0^h (\overline{Q}_{12}\zeta_x + \overline{Q}_{22}\zeta_y + \overline{Q}_{26}\zeta_{xy}) \, [1, z] \, dz \qquad (2.12)$$

Defining the matrices

$$[L] = \begin{pmatrix} a_{11} & b_{11} \\ b_{11} & d_{11} \end{pmatrix} \qquad (2.13)$$

$$[M] = \begin{pmatrix} a_{12} & b_{12} \\ b_{12} & d_{12} \end{pmatrix} \qquad (2.14)$$

and

$$[N] = \begin{pmatrix} a_{22} & b_{22} \\ b_{22} & d_{22} \end{pmatrix} \qquad (2.15)$$

Equations 2.9 and 2.10 take the form of

$$\begin{pmatrix} 0 \\ 0 \end{pmatrix} = [L]\begin{pmatrix} e_x^0 \\ \kappa_x \end{pmatrix} + [M]\begin{pmatrix} e_y^0 \\ \kappa_y \end{pmatrix} - \begin{pmatrix} N_x^T \\ M_x^T \end{pmatrix} \qquad (2.16)$$

and

$$\begin{pmatrix} 0 \\ 0 \end{pmatrix} = [M]\begin{pmatrix} e_x^0 \\ \kappa_x \end{pmatrix} + [N]\begin{pmatrix} e_y^0 \\ \kappa_y \end{pmatrix} - \begin{pmatrix} N_y^T \\ M_y^T \end{pmatrix} \qquad (2.17)$$

From Eq. 2.17 we obtain

$$\begin{pmatrix} e_y^0 \\ \kappa_y \end{pmatrix} = [N]^{-1}\begin{pmatrix} N_y^T \\ M_y^T \end{pmatrix} - [N]^{-1}[M]\begin{pmatrix} e_x^0 \\ \kappa_x \end{pmatrix} \qquad (2.18)$$

and, after substituting from Eq. 2.18 in Eq. 2.16, we obtain

$$\begin{pmatrix} N_x^T \\ M_x^T \end{pmatrix} = [P]\begin{pmatrix} e_x^0 \\ \kappa_x \end{pmatrix} + [M] \, [N]^{-1}\begin{pmatrix} N_y^T \\ M_y^T \end{pmatrix} \qquad (2.19)$$

where

$$[P] = [L] - [M][N]^{-1}[M]$$

Eq. 2.19 defines the thermal force and moment, P^T and M^T respectively, as

$$\begin{pmatrix} P^T \\ M^T \end{pmatrix} = \begin{pmatrix} N_x^T \\ M_x^T \end{pmatrix} - [M][N]^{-1}\begin{pmatrix} N_y^T \\ M_y^T \end{pmatrix} = [P]\begin{pmatrix} e^0_x \\ \kappa_x \end{pmatrix} \tag{2.20}$$

From now on, the thermal force and moment resultants defined in Eq. 2.20 are considered as external forces and moments acting on the composite specimen (Agarwal and Broutman, 1980). The finite element method is used to solve Eq. 2.20 and to obtain the solution for $\epsilon^0_x(x)$ and $\kappa_x(x)$. For bottom element the derivation is the same, except for the limits of integration in Eq. 2.5, 2.8, 2.11 and 2.12.

2.4 Free Edge Problem

In defining the in-plane and transverse displacements for the free edge problem (second phase), Eq. 2.1 remains the same, except for displacement in the y direction, which takes the form of

$$v(y, z) = e_0 y \tag{2.21}$$

where e_0 represents the applied strain in the y direction. Consequently, the strain ϵ_{yy} in Eq. 2.2 is replaced by

$$e_{yy} - e_0 \qquad (2.22)$$

Because the dimension 2b in Figure 2.1 is considered much greater than the dimension 2L, it is assumed that a state of plane strain parallel to the x-z plane exists in the second phase of the free edge problem. The stress-strain relations for the kth layer in this case are

$$\begin{pmatrix} \sigma_{xx} \\ \sigma_{yy} \\ \tau_{zx} \end{pmatrix}_k - \begin{pmatrix} \overline{Q}_{11} & \overline{Q}_{12} & 0 \\ \overline{Q}_{12} & \overline{Q}_{22} & 0 \\ 0 & 0 & \overline{Q}_{55} \end{pmatrix} \cdot \begin{pmatrix} e_{xx} \\ e_0 \\ \gamma_{xz} \end{pmatrix} \qquad (2.23)$$

The in-plane force and moment acting on the beam are shown in Fig. 2.6
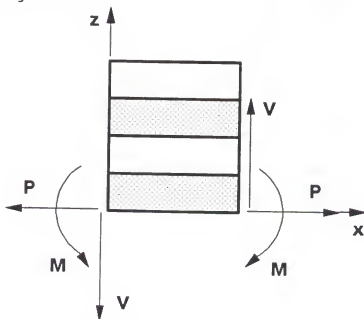
Figure 2.6 Force and moment resultants (top sublaminate)

P, M and V are defined as

$$[P, M, V] = \int_0^h [\sigma_{xx}, z\sigma_{xx}, \tau_{xz}] \, dz \qquad (2.24)$$

or, using the definitions given in Eq. 2.8 and 2.23, as

$$\begin{pmatrix} P \\ M \\ V \end{pmatrix} = \begin{pmatrix} a_{11} & b_{11} & 0 \\ b_{11} & d_{11} & 0 \\ 0 & 0 & a_{55} \end{pmatrix} \begin{pmatrix} e_{xx} \\ e_0 \\ \gamma_{xz} \end{pmatrix} + \begin{pmatrix} P^P \\ M^P \\ 0 \end{pmatrix} \qquad (2.25)$$

where P^P and M^P are the force and moment induced by the applied strain e_0. They are defined as

$$[P^P, M^P] = \int_0^h \overline{Q_{12}} (1, z) \, dz = [a_{12}, b_{12}] \, e_0 \qquad (2.26)$$

The thermal force and moment resultants defined in Eq. 2.20 are added to the problem in the form of external forces, and hence the problem takes the final form of

$$\begin{pmatrix} P \\ M \\ V \end{pmatrix} + \begin{pmatrix} P^T \\ M^T \\ 0 \end{pmatrix} = \begin{pmatrix} a_{11} & b_{11} & 0 \\ b_{11} & d_{11} & 0 \\ 0 & 0 & a_{55} \end{pmatrix} \begin{pmatrix} e_{xx} \\ e_0 \\ \gamma_{xz} \end{pmatrix} + \begin{pmatrix} P^P \\ M^P \\ 0 \end{pmatrix} \qquad (2.27)$$

or

$$\begin{pmatrix} P \\ M \\ V \end{pmatrix} = \begin{pmatrix} a_{11} & b_{11} & 0 \\ b_{11} & d_{11} & 0 \\ 0 & 0 & a_{55} \end{pmatrix} \begin{pmatrix} e_{xx} \\ e_0 \\ \gamma_{xz} \end{pmatrix} - \left(\begin{pmatrix} P^T \\ M^T \\ 0 \end{pmatrix} - \begin{pmatrix} P^P \\ M^P \\ 0 \end{pmatrix} \right) \qquad (2.28)$$

The last equation can be expressed in a more concise form as

$$F = S e - R \qquad (2.29)$$

where S is the stiffness matrix, components of which are

$$[S] = \begin{pmatrix} a_{11} & b_{11} & 0 \\ b_{11} & d_{11} & 0 \\ 0 & 0 & a_{55} \end{pmatrix} \qquad (2.30)$$

and R is the vector that represents the forces and moments induced by the applied strain and by the thermal effects

$$(R) = \begin{pmatrix} P^H \\ M^H \\ 0 \end{pmatrix} - \begin{pmatrix} P^P \\ M^P \\ 0 \end{pmatrix} \qquad (2.31)$$

The vector F refers to the external forces acting on the beam and its components are

$$(F) = \begin{pmatrix} P \\ M \\ V \end{pmatrix} \qquad (2.32)$$

while e is the vector of deformations in the form of

$$(e) = \begin{pmatrix} \epsilon_x^0 \\ \kappa_x \\ \gamma_{zx} \end{pmatrix} \qquad (2.33)$$

Finally, the Equation 2.27 can also be expressed as

$$e = c(F+R) \qquad (2.34)$$

where $c = s^{-1}$ and is the compliance matrix.

2.5 Finite Element Solution

The Finite Element Method is used to solve Eq. 2.29, and a beam finite element with offset nodes is selected to model the problem. The derivation of this specific beam finite element was done by Sankar (1989). The finite element has two nodes and three degrees of freedom (u, ψ and w) at each node. The nodal forces and moment for the ith node are denoted by p_i, m_i and v_i. In the present study a slightly different method is used to derive the stiffness matrix.

The average force and moment resultants (P, M and V) at the center of the element are given by

$$\begin{pmatrix} P \\ M \\ V \end{pmatrix} \quad \begin{pmatrix} (p_2 - p_1) / 2 \\ (m_2 - m_1) / 2 \\ (v_2 - v_1) / 2 \end{pmatrix} \qquad (2.35)$$

The deformations at the center of the element are expressed in terms of the nodal displacements as

$$(e) = \begin{pmatrix} e_x^0 \\ \kappa_x \\ \gamma_{zx} \end{pmatrix} = \begin{pmatrix} (u_2 - u_1) / L \\ (\Psi_2 - \Psi_1) / L \\ (\Psi_2 + \Psi_1) / 2 + (w_2 - w_1) / L \end{pmatrix} \qquad (2.36)$$

where L is the element length.

The beam finite element forces and degrees of freedom are shown in Fig.2.7. By substituting from Eq. 2.33-2.34 into Eq. 2.29, the relations between nodal forces and displacements are obtained in the form of

$$f = k \ q - R \qquad (2.37)$$

where the vectors of nodal forces (f) and displacements (q) have the following components

$$(q)^T = [u_1, \psi_1, w_1, u_2, \psi_2, w_2] \qquad (2.38)$$
$$(f)^T = [p_1, m_1, v_1, p_2, m_2, v_2]$$

The vector R and its components are defined by Eq. 2.20, 2.26 and 2.31. The elements of the stiffness matrix k are

$$[K] = \begin{pmatrix} \dfrac{a_{11}}{L} & \dfrac{b_{11}}{L} & 0 & -\dfrac{a_{11}}{L} & -\dfrac{b_{11}}{L} & 0 \\[2mm] \dfrac{b_{11}}{L} & (\dfrac{d_{11}}{L} + \dfrac{a_{55}L}{4}) & -\dfrac{a_{55}}{2} & -\dfrac{b_{11}}{L} & (-\dfrac{d_{11}}{L} + \dfrac{a_{55}L}{4}) & \dfrac{a_{55}}{2} \\[2mm] 0 & -\dfrac{a_{55}}{2} & \dfrac{a_{55}}{L} & 0 & -\dfrac{a_{55}}{L} & -\dfrac{a_{55}}{L} \\[2mm] -\dfrac{a_{11}}{L} & -\dfrac{b_{11}}{L} & 0 & \dfrac{a_{11}}{L} & \dfrac{b_{11}}{L} & 0 \\[2mm] -\dfrac{b_{11}}{L} & (-\dfrac{d_{11}}{L} + \dfrac{a_{55}L}{4}) & -\dfrac{a_{55}}{2} & \dfrac{b_{11}}{L} & (\dfrac{d_{11}}{L} + \dfrac{a_{55}L}{4}) & -\dfrac{a_{55}}{2} \\[2mm] 0 & \dfrac{a_{55}}{L} & -\dfrac{a_{55}}{L} & 0 & -\dfrac{a_{55}}{2} & \dfrac{a_{55}}{L} \end{pmatrix}$$

$$(2.39)$$

2.6 The Finite Element Models

Fig. 2.3 and 2.4 show the models used in modeling the free edge delaminations. They consist of two sublaminates above and below the delamination plane. The assumptions are that the delamination plane is the weakest plane in the material and that there is no frictional resistance against sliding of the sublaminates. The first assumption means that the crack will propagate along the delamination plane, without crack branching.

In the uncracked region, the top and bottom portions of the beam are connected by common nodes, when calculating the strain energy release rate (Fig. 2.3), and by spring elements, when predicting the stress ahead of the crack (Fig. 2.4).
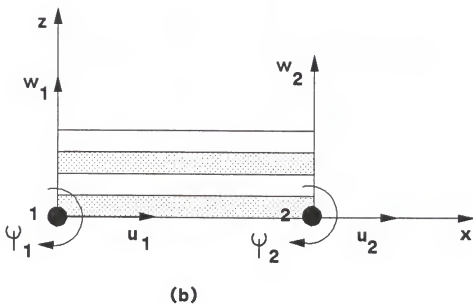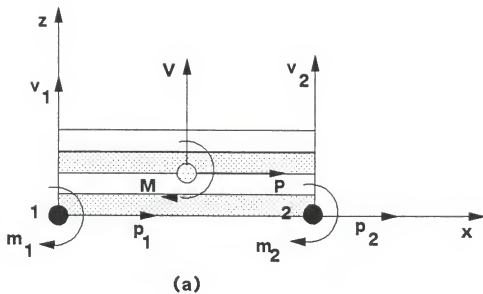
Figure 2.7 Force and degrees of freedom
(a) Nodal and average forces (b) Degrees of freedom

2.7 Strain Energy Release Rate

In the calculation of the strain energy release rate (G), one rigid element is placed in the tip of the crack connecting both sublaminates (Fig. 2.3). The rigid element has nine degrees of freedom. Apart from the three displacements at each node, the three generalized forces, F_t, transmitted by the rigid element are also considered as unknown degrees of freedom. The constraint equations corresponding to the rigid element are

$$\begin{pmatrix} F_1 \\ F_2 \\ 0 \end{pmatrix} = \begin{pmatrix} 0_3 & 0_3 & -I_3 \\ 0_3 & 0_3 & I_3 \\ -I_3 & I_3 & 0_3 \end{pmatrix} \begin{pmatrix} q_1 \\ q_2 \\ F_t \end{pmatrix} \qquad (2.40)$$

where F_1 and F_2 are the nodal forces at nodes 1 and 2 and q_1 and q_2 are the nodal displacements. The symbol 0_3 represents the 3x3 null matrix and I_3 the 3x3 identity matrix.

Considering a zero volume path surrounding the crack tip as shown in Fig. 2.8, the expression for the J-integral relative to two-dimensional states can be found in Hellan (1984) as

$$J = \int_\Gamma \left(W dx_2 - p_i \frac{\partial u_i}{\partial x_1} ds \right) \qquad (2.41)$$

where

$$p_i = n_j \sigma_{ji} \qquad i = 1,2$$

For the present case, and considering the path Γ very thin (zero-volume), the Eq.2.41 takes the form of

$$J = \int_{\Gamma} W \, dz - \int_{\Gamma} n_x \sigma_{xx} u_{,x} ds - \int_{\Gamma} n_x \tau_{zx} w_{,x} ds \qquad (2.42)$$

where W is the strain energy density and is defined as

$$W = \frac{1}{2} (\sigma_{xx} \epsilon_{xx} + \sigma_{yy} \epsilon_{yy} + \tau_{zx} \gamma_{zx}) \qquad (2.43)$$

The path Γ has four segments, one in each sublaminate behind and ahead of the crack tip (Fig. 2.8). The values of n_x (unit vector normal to the path) and ds for each element are:

Elements 1 and 4: $n_x = -1$; ds $= -dz$

Elements 2 and 3: $n_x = 1$; ds $= dz$

Considering the Element 1 in Fig.2.8 we have:

$$J_1 = -\int_0^h W \, dz + \int_0^h \sigma_{xx} u_{,x} dz + \int_0^h \tau_{zx} w_{,x} dz \qquad (2.44)$$

where the subscript stands for the element number.

The first term of the right hand side of Eq.2.44 is defined by using Eq.2.43 and the stress-strain relations given in Eq.2.23 as

$$\int_0^h W dz = \frac{1}{2} \int_0^h (\overline{Q}_{11} \epsilon_{xx}^2 + 2 \overline{Q}_{12} \epsilon_{xx} e_o + \overline{Q}_{22} e_o^2 + \overline{Q}_{55} \gamma_{zx}^2) \, dz \qquad (2.45)$$
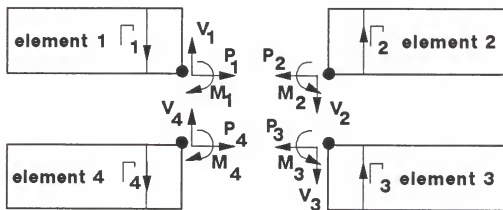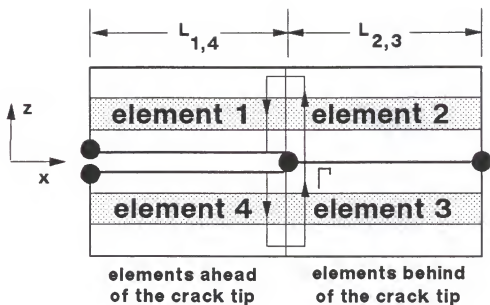
Figure 2.8 Zero-volume path for J-integral

From the definition of the stiffness coefficients and Eq. 2.30 and 2.33 we obtain the following relation

$$e^T S e = \int\limits_0^h (\overline{Q}_{11}e_{xx}^2 + \overline{Q}_{55}\gamma_{zx}^2)\, dz \qquad (2.46)$$

Therefore, the Eq.2.45 can be modified and expressed as

$$\int\limits_0^h W dz = \frac{1}{2} e_1^T S e_1 + a_{12}e_0 e_{xx} + \frac{1}{2} a_{22}e_0^2 \qquad (2.47)$$

The second term of the right hand side of Eq.2.44 is modified in a similar way to what has been done for the first term.

$$\int\limits_0^h \sigma_{xx}u_{,x}dz = \int\limits_0^h (\overline{Q}_{11}e_{xx}^2 + \overline{Q}_{12}e_{xx}e_o)\, dz \qquad (2.48)$$

or

$$\int\limits_0^h \sigma_{xx}u_{,x}dz = \int\limits_0^h (\overline{Q}_{11}e_{xx}^2 + \overline{Q}_{12}e_{xx}e_o + \overline{Q}_{55}\gamma_{zx}^2 - \overline{Q}_{55}\gamma_{zx}^2)\, dz \qquad (2.49)$$

Finally,

$$\int\limits_0^h \sigma_{xx}u_{,x}dz = e_1^T S e_1 + a_{12}e_0 e_{xx} - a_{55}\gamma_{zx}^2 \qquad (2.50)$$

The third term of Eq. 2.42 is

$$\int_0^h \tau_{zx} w_{,x} dz = V_1 \psi_1 \qquad (2.51)$$

where V_1 and ψ_1 are the shear force resultant (Eq. 2.24) and the rotation at the crack tip, respectively, for the element number 1.

Substituting Eq. 2.48, 2.50 and 2.51 into Eq. 2.44 we obtain

$$J_1 = \frac{1}{2} e_1{}^T S e_1 + U_c \qquad (2.52)$$

where U_c is a energy term defined by

$$U_c = -\frac{1}{2} a_{22} e_0{}^2 - a_{55} \gamma_{zx}{}^2 \qquad (2.53)$$

Similar expressions can be obtained for the other elements in the form of

$$\begin{aligned} J_2 &= -\frac{1}{2} e_2{}^T S e_2 - U_c \\ J_3 &= -\frac{1}{2} e_3{}^T S e_3 - U_c \\ J_4 &= \frac{1}{2} e_4{}^T S e_4 + U_c \end{aligned} \qquad (2.54)$$

For linear elastic fracture, the J-integral is equivalent to the energy release rate (Hellan, 1984). This is valid for fractures in brittle composite materials, where the plastic zone in the vicinity of the crack is negligible. Hence,

$$G = J = J_1 + J_2 + J_3 + J_4 =$$
$$-\frac{1}{2} (e_1^T S e_1 + e_4^T S e_4 - e_2^T S e_2 - e_3^T S e_3) \qquad (2.55)$$

The Eq.2.55 can be calculated in a more convenient form,

$$G = \frac{1}{2} (F_1^T c_t F_1 + F_4^T c_b F_4 - F_2^T c_t F_2 - F_3^T c_b F_3) \qquad (2.56)$$

where the forces F_i (i=1,2,3,4) are calculated from the finite element solution, and so are the compliance matrices c_t and c_b from the input data.

The elements 2 and 3 are in the uncracked region, and so, they are under the same deformations. We thus obtain the relations,

$$e_2 = e_3$$
$$c_t F_2 = c_b F_3 \qquad (2.57)$$

Substituting the last equation, and also the equilibrium relations ($F_1 + F_4 = F_2 + F_3$), in Eq. 2.56 we obtain

$$G = \frac{1}{2} (F_1^T c_t - F_4^T c_b) (F_1 - F_2) \qquad (2.59)$$

or, using again the equilibrium relations,

$$G = \frac{1}{2} (F_1 - F_2)^T (c_t + c_b) (F_1 - F_2) \qquad (2.60)$$

Actually, $(F_1 - F_2)$ is the force transmitted by the rigid element, F_r, between bottom and top crack tip nodes. Therefore, the strain energy release rate (G) can be expressed in a more convenient form as

$$G = \frac{1}{2} F_r^T (c_t + c_b) F_r \qquad (2.61)$$

where F_r are considered unknown degrees of freedom and part of the finite element solution of the problem (Eq. 2.40).

One can also evaluate the value of the strain energy release rate using a method analogous to the virtual crack closure method in two-dimensional fracture problems (Hellan, 1984). In this method, the energy necessary to "close" the crack is equal to the energy release rate.

In Fig. 2.9, as the crack propagates, the crack tip Nodes 1 and 2 have displacements Δ_1 and Δ_2, respectively, and the crack tip moves to Node 5. If the length of the elements behind the crack tip is sufficiently small, ΔL, then the crack opening, $(\Delta q_1 - \Delta q_2)$, will be approximately equal to the difference in displacements of Nodes 3 and 4, $(\Delta q_3 - \Delta q_4)$. Therefore, the problem is analyzed considering the displacements of Nodes 1 and 2 as the tip displacements of cantilever beams of length ΔL under applied forces F_r on each beam. For very short cantilever beams (thickness/length $\ll 1$)
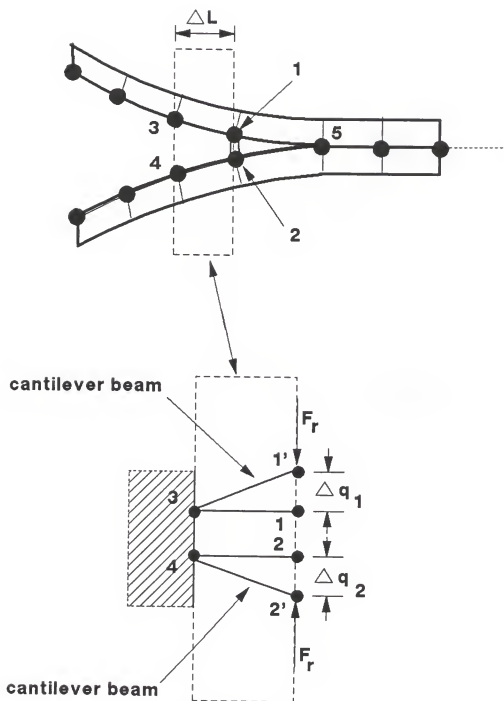
Figure 2.9 Crack-closure method

the tip deflections (q_{tip}) can be calculated using the expression

$$q_{tip} = L [c] F \qquad (2.62)$$

where L and F are the beam length and the forces applied at the tip of the beam, respectively, and c is the compliance matrix. In the present case,

$$\Delta q_1 = \Delta L c_t F_r \\ \Delta q_2 = -\Delta L c_b F_r \qquad (2.63)$$

or

$$\frac{\Delta q_1 - \Delta q_2}{\Delta L} = (c_t + c_b) F_r \qquad (2.64)$$

Substituting the last equation in Eq. 2.61 gives

$$G = \frac{1}{2 \Delta L} F_r{}^T (\Delta q_1 - \Delta q_2) \qquad (2.65)$$

In this equation, the displacements in the tip nodes and the forces in the rigid element are part of the finite element solution.

In the present study, the strain energy release rate was calculated by three different methods. These methods are represented by Eq.2.56, 2.61 and 2.64, and the results obtained from the three equations are in very good agreement.

2.8 Stresses Ahead of the Crack

In evaluating the stresses ahead of the crack tip, the uncracked region was connected by discrete spring elements (Fig. 2.4). The stress ahead of the crack in the i_{th} element was obtained by

$$\sigma_i = \frac{V_i}{\Delta L_i b} \qquad (2.66)$$

where V and L are the vertical force in the spring element and the length of the element, respectively. The vertical forces are obtained from the Finite Element solution of the problem, and the element lengths are part of the input data.

The determination of the spring constant for the spring elements is of significant importance in appropriately modeling the problem. The spring constants are derived from the change in thickness of a beam subjected to transverse forces. The exact change in thickness is obtained from the two dimensional elasticity theory (Timoshenko, 1970). In the first step, just the top part of the beam is considered and it is represented in Fig. 2.10. From the elasticity theory we have, for this case

$$e_{yy} = -\frac{3q}{4c^3 E^*} \ (\frac{1}{3} \ y^3 - c^2 y + \frac{2}{3} c^3) \qquad (2.67)$$
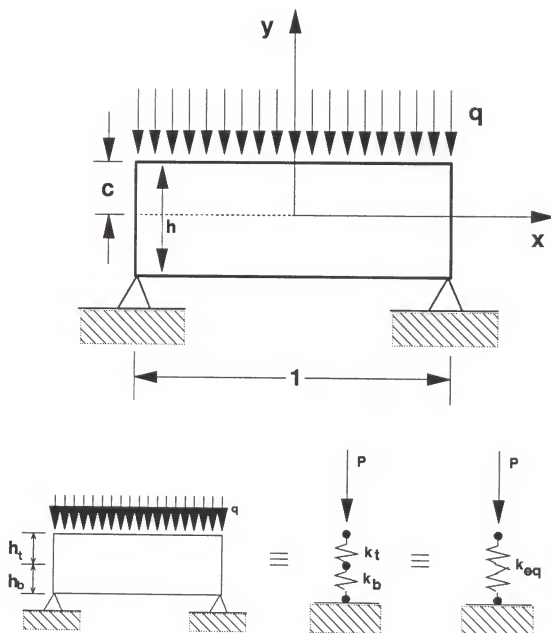
Figure 2.10 Model for spring constant calculation

where E^* is defined as

$$E^* = C_{33} = \frac{1 - \nu_{12}\nu_{21}}{E_1 E_2 \Delta} \qquad (2.68)$$

and

$$\Delta = \frac{1 - \nu_{12}\nu_{21} - \nu_{23}\nu_{32} - \nu_{31}\nu_{13} - 2\nu_{21}\nu_{32}\nu_{13}}{E_1 E_2 E_3} \qquad (2.69)$$

The vertical displacement (v) is obtained by integrating the deformation ϵ_{yy} in the y direction. The result is

$$v = \int e_{yy} dy = -\frac{3q}{4 c^3 E^*} \left(\frac{y^4}{12} - \frac{c^2 y^2}{2} + \frac{2}{3} c^3 y \right) + C_1 \qquad (2.70)$$

where C_1 is a constant.

From Eq. 2.70 the displacements at the positions y=-c and y=0 are determined as

$$v(-c) = \frac{13}{16} \frac{qc}{E^*} + C1 \qquad (2.71)$$
$$v(0) = C1$$

The relative displacement between these two particular positions is

$$v_R = v(-c) - v(0) = \frac{13}{16} \frac{qc}{E^*} \qquad (2.72)$$

For a beam with unit area we have that P = q. In the present case, c is equal to half the thickness of the beam (c = h/2). Therefore Eq. 2.72 is rewritten as

$$P = \frac{32 E^* v_R}{13 h} \tag{2.73}$$

For a spring model we have

$$P = k \, v_R \tag{2.74}$$

where k is the spring constant.

By comparing between Eqs. 2.73 and 2.74 we have the value for the spring constant per unit length considering just the top part of the element.

$$k = \frac{32 E^*}{13 h} \tag{2.75}$$

Considering both parts, top and bottom, we have two springs placed in a series arrangement (Fig. 2.10). The spring constant equivalent (k_{eq}) to this kind of arrangement is given by

$$k_{eq} = \frac{k_t k_b}{k_t + k_b} \tag{2.76}$$

where the subscripts t and b stand for top and bottom respectively. Substituting Eq. 2.80 in the last equation we obtain the final expression for the spring constant used in the present study

$$k_{eq} = \frac{32\,E^*}{13\,(h_t + h_b)} \qquad (2.77)$$

2.9 Numerical Results

Some results from the investigation of strain energy release rate and the interlaminar stresses in a free edge specimen can be found in Whitney (1987), (Pagano, 1989) and Raju (1986). These researchers computed results for the same composite specimen. The present study uses the same specimen to make the comparison easier.

The free-edge specimen width to thickness ratio (b/h) is 25 (Fig 2.11-2.16), which is typical for conventional edge delamination test (EDT) specimens. Considering a coordinate system where x_1 and x_2 are parallel and transverse to the fibers respectively, and x_3 is through the thickness, the ply properties have the following relations and values:

$$E_1/E_2 \;\; = 14 \qquad\qquad E_2/E_3 \;\; = 1$$

$$G_{12}/E_2 = 0.533 \qquad\qquad G_{23}/E_2 = 0.323$$

$$v_{12} = 0.3 \qquad\qquad v_{23} = 0.55$$

$$\alpha_1 = -9\ E\text{-}07/°C \qquad\qquad \alpha_2 = \alpha_3 = 23\ E\text{-}06/°C$$

$$\beta_1 = 0 \qquad\qquad \beta_2 = \beta_3 = 5560\ E\text{-}06/\%$$

where E_i is the elastic moduli in the ith direction, G_{ij} is the shear modulus in the $x_i - x_j$ plane and ν_{ij} are the Poisson's ratios. Finally, the thermal expansion coefficients and the moisture swelling coefficient in the x_i direction are denoted by α_i and β_i, respectively. These properties and relations among them are typical of current high performance graphite/epoxy unidirectional composites.

The specimens considered in the present study have the following lay-ups:

Specimen A: $[90_3/0_3]_s$ Specimen B: $[-60/60_2/-60/0_2]_s$

Specimen C: $[-45/45_2/-45/0_2]_s$ Specimen D: $[0_2/-60/60_2/-60]_s$

A reasonable stress-free temperature for standard graphite/epoxy laminates is 138°C (280°F) (Whitney, 1987). Assuming 21°C (70°F) as the room temperature, the difference in temperature (ΔT) that causes residual stresses in the plies is equal to -117°C (210°F).

The critical axial strains (e_0) experimentally determined in edge delamination tests are 0.3% for angle-ply laminates, and 1% for the special case of a bidirectional class of laminates (Whitney, 1986). Therefore, these values of strains are used in the numerical examples.

2.9.1 Strain energy release rate

The normalized strain energy release rate, G_N, is given by

$$G_N = \frac{G}{E_2 h \, e_0^2} \qquad (2.78)$$

In the present study the energy release rate was calculated using Eqs. 2.56, 2.61 and 2.65. The results obtained from these three methods were in good agreement and they are refered to as "Present" in Table 2.1. Comparison of the results from the present study with available results is also present in Table 2.1. The relative differences between the results from the offset-node method and each of the other three approaches are shown in Table 2.2.

From Tables 2.1 and 2.2 it may seen that the present results compare very well with Raju (1986), whereas the comparison with the other two methods is not good in a few cases. It should be mentioned that of the three methods we compared with, Raju (1986) used a detailed finite element analysis.

2.9.2 Stress ahead of the crack

The interlaminar stresses ahead of the crack tip are evaluated using spring elements in the uncracked region of the specimen. The spring constant for these elements is calculated by Eq. 2.77 and found to be equal to 300×10^9 N/m .

Table 2.1 Comparison of strain energy release rate values obtained from different methods.

LAMINATE	ε (%)	ΔT	WHITNEY	PAGANO	RAJU	PRESENT
$(-60/60_2,-60,0_2)_s$	0.3	0.	1.300	1.300	1.2506	1.3000
	0.3	-117.	1.700	2.000	1.9551	2.0580
$(0_2,-60,60_2,-60)_s$	0.3	0.	1.300	–	1.2700	1.3000
	0.3	-117.	1.000	–	0.6700	0.7160
$(90_3,0_3)_s$	1.0	0.	0.016	0.016	0.0155	0.0156
	1.0	-117.	0.077	0.045	0.0605	0.0650
$(-45,45_2,-45,0_2)_s$	0.3	0.	0.770	0.770	0.7285	0.7440
	0.3	-117.	0.800	0.980	0.9194	0.8640

Table 2.2 Relative difference (%) between the results from present method and other methods.
Relative difference=100 x (present method - other's) / other's

LAMINATE	ε (%)	ΔT	WHITNEY	PAGANO	RAJU
$(-60/60_2,-60,0_2)_s$	0.3	0.	0.0	0.0	4.0
	0.3	-117.	21.6	2.9	5.3
$(0_2,-60,60_2,-60)_s$	0.3	0.	0.0	–	2.4
	0.3	-117.	-28.4	–	6.9
$(90_3,0_3)_s$	1.0	0.	2.5	2.5	0.6
	1.0	-117.	-15.6	44.4	0.0
$(-45,45_2,-45,0_2)_s$	0.3	0.	-3.4	-3.4	2.1
	0.3	-117.	8.0	-11.8	-6.0

Fig. 2.11-2.15 show the results for peel stresses for different laminate configurations, with and without thermal effects. From the results we find that the effect of residual thermal stresses is to cause increase in the maximum peel stress at the free edge. The effect is significant for specimen A ($[90_3/0_3]$) and less significant for specimen C ($[-45/45_2/-45/0_2]_s$). In Fig. 2.11 the stress distribution is compared with Whitney (1987) for $\Delta = 0°C$ and $\Delta = -117°C$ for the specimen B ($[-60/60_2/-60/0_2]_s$). The agreement is excellent. For the bidirectional laminates, specimen A, the influence of temperature can be better appreciated in Fig.2.15, where the temperature variation goes from zero to -120°C in increments of -30°C.

Besides thermal stresses, some studies on effect of moisture absorption on the free edge stresses were also performed. In fact, the analysis procedure is similar except that $\alpha \Delta T$ has to be replaced by $\beta \Delta H$, where β is the swelling coefficient and ΔH represents the variation in the moisture concentration. Fig. 2.16 shows the influence of the moisture level variation on specimen A. The moisture level was allowed to vary from 0% to 1.2% of the laminate weight, which reflects feasible conditions. This result agrees with those obtained by Armanios and Badir (1989). Unlike the thermal stresses, the residual moisture tends to decrease the interlaminar stress close to the crack front.

2.9.3 Conclusions

The residual thermal stress tends to increase the total energy release rate and the interlaminar stress at the tip of the crack, while the residual moisture alleviates these effects.

The results obtained from the offset nodes method are very close to those obtained by Whitney (1987), Pagano(1989), Raju(1986) and Armanios and Badir (1989) using different methods. Therefore, the present offset-node method is a good method to predict the energy release rate and stresses ahead of the crack tip in the free-edge problems. The present finite element method has the facility to model any type of geometry, loading and boundary conditions, and avoids renumbering the nodes and elements as the crack propagates.

The offset node method can be used in studying dynamic delamination, and can be extended to problems of sublaminate buckling and delaminations in composite plates.
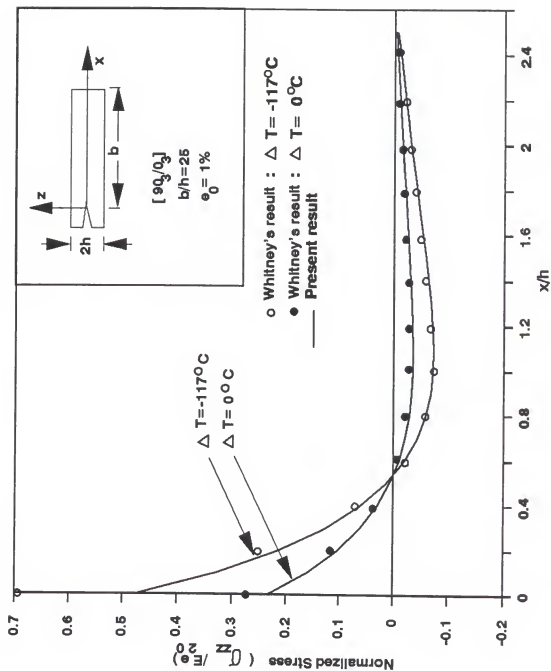
Figure 2.11 Stresses ahead of the crack tip for specimen A
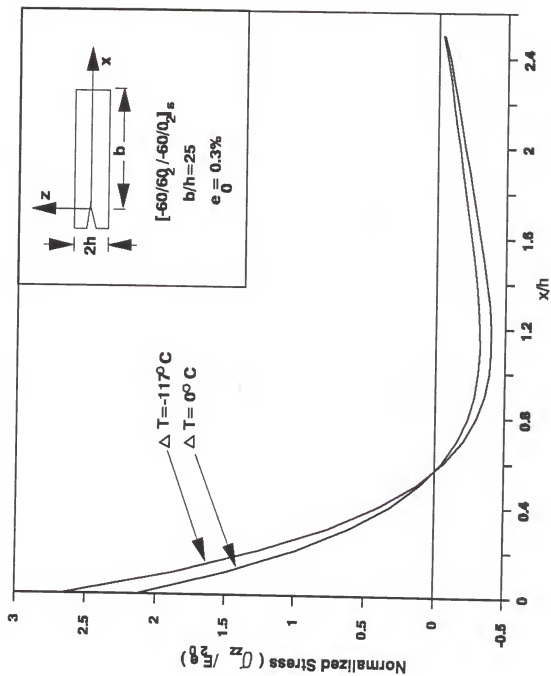
Figure 2.12 Stresses ahead of the crack tip for specimen B
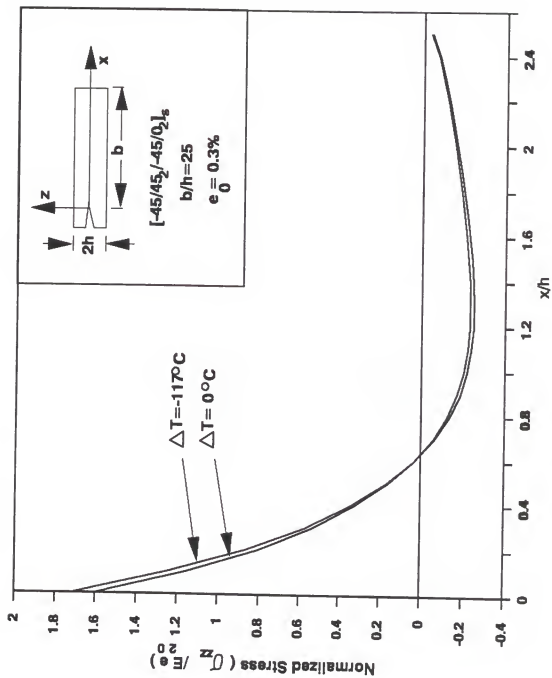
Figure 2.13 Stresses ahead of the crack tip for specimen C
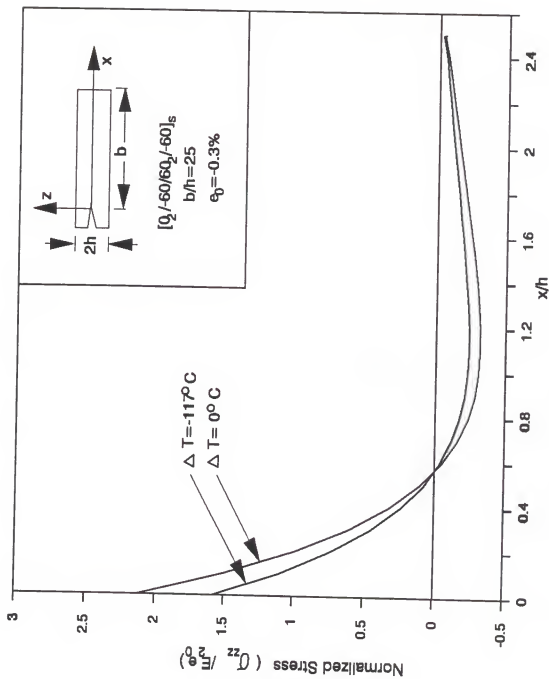
Figure 2.14 Stresses ahead of the crack tip for specimen D
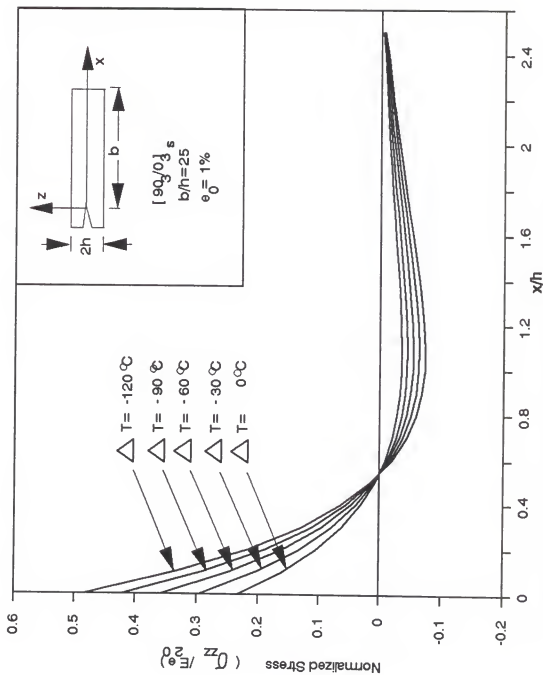
Figure 2.15 Influence of temperature variation
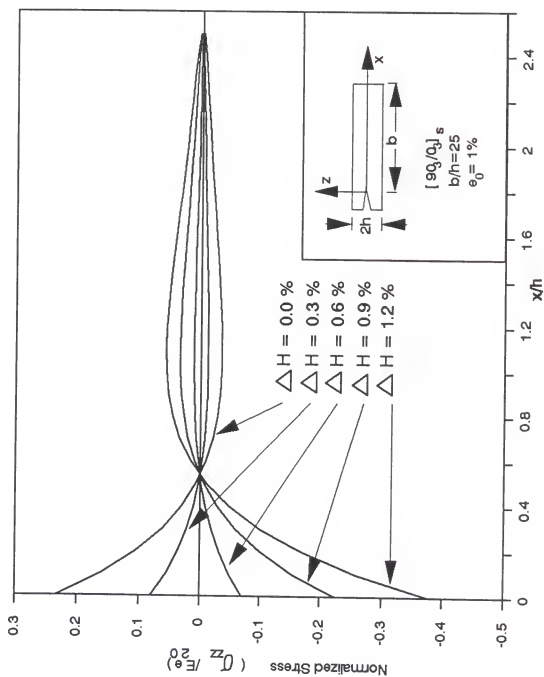
Figure 2.16 Influence of moisture level variation

CHAPTER 3

MODELING DELAMINATION IN COMPOSITE BEAMS
AND APPLICATION TO TORSION PROBLEM

3.1 Introduction

The application of composite materials is increasing day by day. Not only traditional areas like aerospace and automobile structures, but also several other areas, such as robotics, marine industries and medical devices and prostheses, have shown that the application of composite materials is major factor in the improvement of their mechanical structures.

The advances in the manufacturing processes of composite materials, the development of new matrices and fibers, and the progress in methods for study of the mechanical behavior of composites have been made it possible for the composite materials to replace traditional materials in several mechanical structures. Usually composite materials are considered as a possible and adequate solution whenever the weight savings and the capability of "tailoring" the material in according to specific needs are more critical than the costs.

As the use of composite materials in structural applications increases, there is more need for structural

analysis. Unlike an isotropic beam, stretching a laminated composite beam can produce bending, shear and twisting in addition to the extensional deformation. The coupling among the modes of deformation is the major obstacle to precisely modeling the mechanical behavior of beam like composite structures.

In the present chapter, a new and efficient method to analyze delaminations in laminated composite beams is presented. The equations of equilibrium were derived by Sankar (1991) from the classical shear deformable laminated plate theory (Whitney, 1987). The equilibrium equations are assumed to be satisfied in an average sense over the width of the beam. From this assumption results a new set of force and moment resultants, which amplify the possibilities for modeling beams under different loading conditions, including torsion. The equilibrium equations are derived from the Minimum Potential Energy Principle.

In the present study a new offset beam finite element is developed for modeling the problem. Initially, the capability of the new finite element in modeling the problem is verified by solving the problem of a cantilever beam under different end loading conditions. The results are compared with those from beam theory solutions found in Timoshenko (1970), Reismann and Pawlik (1980), Whitney (1987) and Sankar (1991). Next, the strain energy release rate for a delaminated specially orthotropic cantilever beam under torsion is

calculated. The delamination is considered to be at the middle-plane of the beam. The results for G from the finite element method are compared with analytical solutions of the problem. The effect of position of delamination on the strain energy release rate values is presented. Finally, the problems of a specially orthotropic and a quasi-isotropic simply supported delaminated beam under a transverse force is considered. The strain energy release rate values for various positions of the delamination are computed by using the finite elements developed in the present study. The results will be useful in explaining delamination propagation in composite beams due to quasi-static impact.

3.2 Beam Equations

Considering the laminated beam shown in Fig. 3.1, the Shear Deformation Theory (Whitney, 1987) for laminated plates assumes the displacement field as

$$
\begin{aligned}
u(x,y,z) &= u_0(x,y) + z\psi_x(x,y) \\
v(x,y,z) &= v_0(x,y) + z\psi_y(x,y) \\
w(x,y,z) &= w_0(x,y)
\end{aligned}
\tag{3.1}
$$

where u_0, v_0 and w_0 are the displacements in the middle plane of the plane in the x, y and z directions, respectively, and so, are ψ_x and ψ_y with respect to the rotations about the X and Y axes.

All five displacements and rotations in equation 3.1 can be expanded as a Taylor series, in the direction of the width
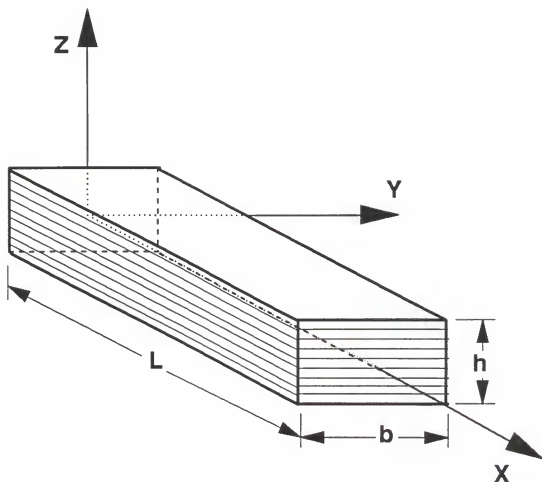
Figure 3.1 Laminated composite beam

of the plate. If just the first order terms of this series are retained, the displacements and rotations can be expressed in the form of

$$
\begin{aligned}
u_0(x,y) &= U(x) + yF(x) \\
v_0(x,y) &= V(x) + yG(x) \\
w(x,y) &= W(x) + y\theta(x) \\
\psi_x(x,y) &= \phi(x) + y\alpha(x) \\
\psi_y(x,y) &= \Psi(x) + y\beta(x)
\end{aligned}
\tag{3.2}
$$

The displacement field is now represented in terms of ten functions of the x coordinate.

$$
\begin{aligned}
u(x,y,z) &= U(x) + yF(x) + z\phi(x) + yz\alpha(x) \\
v(x,y,z) &= V(x) + yG(x) + z\Psi(x) + yz\beta(x) \\
w(x,y,z) &= W(x) + y\theta(x)
\end{aligned}
$$

From the beam theory, we assume that there is no deformation in cross sections normal to the x direction ($\epsilon_{zz}=0$, $\epsilon_{yy}=0$ and $\gamma_{yz}=0$). From this assumption and Eq. 3.3 results

$$
e_{yy} = G(x) + z\beta(x) = 0 \tag{3.4}
$$

and

$$
\gamma_{yz} = \psi(x) + y\beta(x) + \theta(x) = 0 \tag{3.5}
$$

From equation 3.4 and 3.5 we obtain that

$$
\begin{aligned}
G(x) &= 0 \\
\beta(x) &= 0 \\
\Psi(x) &= -\theta(x)
\end{aligned}
\tag{3.6}
$$

The displacement field can now be represented in terms of seven functions of the x coordinate, instead of the ten functions used before.

$$
\begin{aligned}
u(x,y,z) &= U(x) + yF(x) + z\phi(x) + yz\alpha(x) \\
v(x,y,z) &= V(x) - z\theta(x) \\
w(x,y,z) &= W(x) + y\theta(x)
\end{aligned}
$$

Denoting the differentiation with respect to x by a prime, we represent the deformation field from Eq. 3.7 as

$$\begin{pmatrix} \varepsilon_{xx} \\ \gamma_{xy} \\ \gamma_{zx} \end{pmatrix} = \begin{pmatrix} U' + yF' \\ F + V' \\ (\phi + W') + y(\alpha + \theta') \end{pmatrix} + z \begin{pmatrix} \phi' + y\alpha' \\ \alpha - \theta' \\ 0 \end{pmatrix} = \begin{pmatrix} \varepsilon_x^{\,0} \\ \gamma_{xy}^{\,0} \\ \gamma_{zx}^{\,0} \end{pmatrix} + z \begin{pmatrix} \kappa_x \\ \kappa_{xy} \\ 0 \end{pmatrix} \tag{3.8}$$

The deformation field can also be expressed as

$$E = \overline{E} + y\hat{E} \tag{3.9}$$

where

$$(E) = \begin{pmatrix} \varepsilon_{x0} \\ \gamma_{xy0} \\ \kappa_x \\ \kappa_{xy} \\ \gamma_{zx} \end{pmatrix} ; \quad (\overline{E}) = \begin{pmatrix} U' \\ V' + F \\ \phi' \\ \alpha - \theta' \\ \phi + W' \end{pmatrix} ; \quad (\hat{E}) = \begin{pmatrix} F' \\ 0 \\ \alpha' \\ 0 \\ \alpha + \theta' \end{pmatrix} \tag{3.10}$$

From the constitutive relations the stresses developed in the kth layer are given by

$$\begin{pmatrix} \sigma_{xx} \\ \tau_{xy} \end{pmatrix} = [\overline{Q}] \begin{pmatrix} \varepsilon_{x0} \\ \gamma_{xy0} \end{pmatrix} + z[\overline{Q}] \begin{pmatrix} \kappa_x \\ \kappa_{xy} \end{pmatrix} \tag{3.11}$$

and

$$\tau_{zx} = \overline{Q}_{55}(\phi + W') + y\,\overline{Q}_{55}(\alpha + \theta') \tag{3.12}$$

where

$$[\overline{Q}] = \begin{pmatrix} \overline{Q}_{11} & \overline{Q}_{12} & \overline{Q}_{16} \\ \overline{Q}_{12} & \overline{Q}_{22} & \overline{Q}_{26} \\ \overline{Q}_{16} & \overline{Q}_{26} & \overline{Q}_{66} \end{pmatrix} \tag{3.13}$$

The terms Q_{ij} in Eq. 3.13 are stiffness terms and can be found in Whitney (1987).

By definition, the force (N) and moment (M) acting on the laminate are

$$(N_x, M_x) = \int_{-\frac{h}{2}}^{\frac{h}{2}} \sigma_{xx}[1, z]\, dz$$

$$(N_{xy}, M_{xy}) = \int_{-\frac{h}{2}}^{\frac{h}{2}} \tau_{xy}[1, z]\, dz \qquad (3.14)$$

$$V_x = \int_{-\frac{h}{2}}^{\frac{h}{2}} \tau_{xz}\, dz$$

and they are shown in Fig. 3.2.

The stiffness coefficient terms are defined as

$$(A_{ij}, B_{ij}, D_{ij}) = \int_{-\frac{h}{2}}^{\frac{h}{2}} \overline{Q}_{ij}[1, z, z^2]\, dz \qquad (3.15)$$

By using equations 3.9-13 and the definition of stiffness coefficients, the Eq. 3.14 can be written in a more simplified form as

$$F = C(\overline{E} + y\hat{E}) \qquad (3.16)$$

where

$$(F)^T = (N_x, N_{xy}, M_x, M_{xy}, V_x) \qquad (3.17)$$
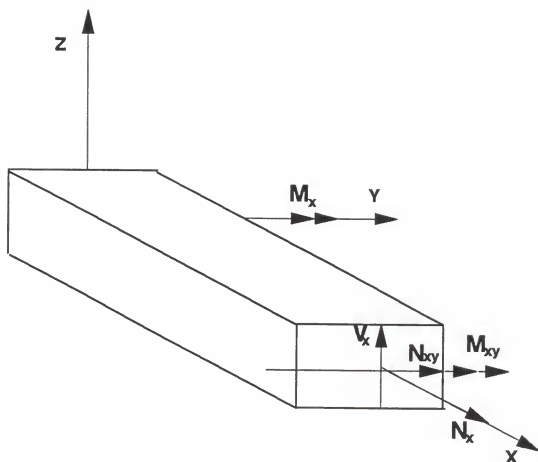
Figure 3.2 Force and moment resultants

and the matrix C is formed with the following stiffness coefficient terms

$$[C] = \begin{pmatrix} A_{11} & A_{16} & B_{11} & B_{16} & 0 \\ A_{16} & A_{66} & B_{16} & B_{66} & 0 \\ B_{11} & B_{16} & D_{11} & D_{16} & 0 \\ B_{16} & B_{66} & D_{16} & D_{66} & 0 \\ 0 & 0 & 0 & 0 & kA_{55} \end{pmatrix} \qquad (3.18)$$

The factor k presented in term C_{55} is the shear correction factor (Whitney, 1987), and it is considered equal to 5/6 in the present work.

3.3 New Set of Force and Moment Resultants

A new set of force and moment resultants is defined from the integration of the column vector of forces along the width of the beam:

$$\bar{F} = \int_{-\frac{b}{2}}^{\frac{b}{2}} F \, dy \qquad (3.19)$$

and

$$\hat{F} = \int_{-\frac{b}{2}}^{\frac{b}{2}} F \, y \, dy \qquad (3.20)$$

In the two last equations, the vector of forces F is given by equation 3.17, and b is the width of the beam.

Substituting equation 3.16 in Eq. 3.19-3.20, and assuming that the stiffness C of the beam is constant, we obtain

$$\overline{F} = \int_{-b/2}^{b/2} C \, \overline{E} \, dy - b C \overline{E}$$
$$\hat{F} = \int_{-b/2}^{b/2} C \, \hat{E} \, y^2 \, dy - \left(\frac{b^3}{12}\right) C \hat{E}$$

(3.21)

The explicit beam contitutive relations are:

$$[\overline{F}] = \begin{pmatrix} \overline{N}_x \\ \overline{N}_{xy} \\ \overline{M}_x \\ \overline{M}_{xy} \\ \overline{V}_x \end{pmatrix} = b \begin{pmatrix} A_{11} & A_{16} & B_{11} & B_{16} & 0 \\ A_{16} & A_{66} & B_{16} & B_{66} & 0 \\ B_{11} & B_{16} & D_{11} & D_{16} & 0 \\ B_{16} & B_{66} & D_{16} & D_{66} & 0 \\ 0 & 0 & 0 & 0 & k^2 A_{55} \end{pmatrix} \begin{pmatrix} U' \\ V'+F \\ \phi' \\ \alpha-\theta' \\ \phi+W' \end{pmatrix}$$

(3.22)

and

$$[\hat{F}] = \begin{pmatrix} \hat{N}_x \\ \hat{M}_x \\ 0 \\ 0 \\ \hat{V}_x \end{pmatrix} = \left(\frac{b^3}{12}\right) \begin{pmatrix} A_{11} & A_{16} & B_{11} & B_{16} & 0 \\ A_{16} & A_{66} & B_{16} & B_{66} & 0 \\ B_{11} & B_{16} & D_{11} & D_{16} & 0 \\ B_{16} & B_{66} & D_{16} & D_{66} & 0 \\ 0 & 0 & 0 & 0 & k^2 A_{55} \end{pmatrix} \begin{pmatrix} F' \\ \alpha' \\ 0 \\ 0 \\ \alpha+\theta' \end{pmatrix}$$

(3.23)

3.4 Equilibrium Equations

The Principle of Minimum Potential Energy is applied in the derivation of the equilibrium equations. The principle says that of all displacement fields which satisfy the prescribed constraint conditions, the correct state is that which makes the total potential energy of the structure a minimum (Tauchert, 1970). The total potential energy of the structure (π) is obtained from the sum of the strain energy of the beam (ϕ) and the potential of the external force (χ):

$$\pi = \phi + \chi \qquad (3.24)$$

According to the Principle of Minimum Potential Energy,

$$\delta\pi = \delta\phi + \delta\chi = 0 \qquad (3.25)$$

where the symbol δ is the variational operator.

Considering only transverse loading acting on the beam surface in the z-direction, the potential relative to the external loading is given by

$$\chi = -\int\limits_{0}^{L}\int\limits_{-\frac{b}{2}}^{\frac{b}{2}} q(x,y)\, w(x,y)\, dy\, dx \qquad (3.26)$$

where $q(x,y)$ and $w(x,y)$ are the transverse loading and displacement, respectively, and L is the beam length.

Similar to the procedure adopted to define a new set of force resultants in Eqs 3.19-20, the transverse loading is divided into two parts and defined by

$$q(x,y) = \overline{q}(x) + y\, \hat{q}(x) \qquad (3.27)$$

where

$$\overline{q}(x) = \int\limits_{-\frac{b}{2}}^{\frac{b}{2}} q(x,y)\, dy$$
$$\hat{q}(x) = \int\limits_{-\frac{b}{2}}^{\frac{b}{2}} q(x,y)\, y\, dy \qquad (3.28)$$

Substituting the definition of transverse displacement (Eq. 3.7) and transverse loading (Eq. 3.28) in Eq. 3.26 gives the result

$$\chi = -\int_{0}^{L} (\overline{q}(x) W(x) + \hat{q}(x)\theta(x))\ dx \qquad (3.29)$$

From Eq. 3.16, the strain energy per unit area (ϕ_A) of the beam can be derived as

$$\phi_A = \frac{1}{2}\ E^T C E$$
$$= \frac{1}{2}\ (\overline{E}+y\hat{E})^T C (\overline{E}+y\hat{E}) \qquad (3.30)$$

The strain energy per unit length (ϕ_L) is obtained by integrating ϕ_A along the width (b) of the beam

$$\phi_L = \int_{-\frac{b}{2}}^{\frac{b}{2}} \phi_A\ dy$$
$$= \frac{1}{2} \int_{-\frac{b}{2}}^{\frac{b}{2}} (\overline{E}+y\hat{E})^T C (\overline{E}+y\hat{E})\ dy \qquad (3.31)$$

Because

$$\int_{-\frac{b}{2}}^{\frac{b}{2}} \overline{E}^T C \overline{E} y\, dy = 0$$
$$\int_{-\frac{b}{2}}^{\frac{b}{2}} \hat{E}^T C \hat{E} y\, dy = 0 \qquad (3.32)$$

the Eq. 3.31 takes the form of

$$
\begin{aligned}
\phi_L - \frac{1}{2} \int_{-\frac{b}{2}}^{\frac{b}{2}} (\overline{E}^T C \overline{E}) \, dy + \frac{1}{2} \int_{-\frac{b}{2}}^{\frac{b}{2}} (\hat{E}^T C \hat{E}) \, y^2 \, dy \\
- \frac{1}{2} \left(b \overline{E}^T C \overline{E} + \frac{b^3}{12} \hat{E}^T C \hat{E} \right)
\end{aligned}
\tag{3.33}
$$

The total strain energy in the beam is expressed as

$$
\begin{aligned}
\phi - \int_0^L \phi_L \, dx \\
- \frac{1}{2} \int_0^L \left(b \overline{E}^T C E + \frac{b^3}{12} \hat{E}^T C \hat{E} \right) dx
\end{aligned}
\tag{3.34}
$$

The total potential of energy in the whole structure (π) is obtained by substituting the Eq. 3.29 and 3.34 into equation 3.24.

$$
\pi - \frac{1}{2} \int_0^L \left(b \overline{E}^T C \overline{E} + \frac{b^3}{12} \hat{E}^T C \hat{E} - \overline{q}(x) W(x) - \hat{q}(x) \theta(x) \right) dx
\tag{3.35}
$$

Applying the Principle of Minimum Potential Energy we obtain the following equilibrium equations

$$
\begin{aligned}
\frac{\delta \pi}{\delta U} &- \frac{d\overline{N}_x}{dx} = 0 \\
\frac{\delta \pi}{\delta V} &- \frac{d\overline{N}_{xy}}{\delta x} = 0 \\
\frac{\delta \pi}{\delta W} &- \frac{d\overline{V}_x}{dx} + \overline{q} = 0 \\
\frac{\delta \pi}{\delta F} &- \overline{N}_{xy} - \frac{d\hat{N}_x}{dx} = 0 \\
\frac{\delta \pi}{\delta \theta} &- \frac{d(\hat{V}_x - \overline{M}_{xy})}{dx} + \hat{q} = 0 \\
\frac{\delta \pi}{\delta \phi} &- \hat{V}_x - \frac{d\overline{M}_x}{dx} = 0 \\
\frac{\delta \pi}{\delta \alpha} &- \frac{d\hat{M}_x}{dx} - \hat{V}_x - \overline{M}_{xy} = 0
\end{aligned}
\tag{3.36}
$$

Next, from each equilibrium equation in Eq. 3.36 results one corresponding natural boundary condition, which is shown in the next equations as

$$\frac{d\overline{N}_x}{dx} = 0 \qquad\qquad \overline{N}_x \delta U = 0$$

$$\frac{d\overline{N}_{xy}}{\delta x} = 0 \qquad\qquad \overline{N}_{xy} \delta V = 0$$

$$\frac{d\overline{V}_x}{dx} = -\overline{q} \qquad\qquad \overline{V}_x \delta W = 0$$

$$\frac{d\hat{N}_x}{dx} = \overline{N}_{xy} \qquad\qquad \hat{N}_x \delta F = 0 \qquad\qquad (3.37)$$

$$\frac{d(\hat{V}_x - \overline{M}_{xy})}{dx} = -\hat{q} \qquad (\hat{V}_x - \overline{M}_{xy})\, \delta\theta = 0$$

$$\frac{d\overline{M}_x}{dx} = \overline{V}_x \qquad\qquad \overline{M}_x \delta\phi = 0$$

$$\frac{d\hat{M}_x}{dx} = \hat{V}_x + \overline{M}_{xy} \qquad \hat{M}_x \delta\alpha = 0$$

By using Eqs. 3.22-23, the new set of force and moment resultants can be expressed in terms of seven unknown functions: U, V, W, F, ϕ, α and θ. Substituting for the resultants in terms of displacements in the equilibrium equations 3.37 results in a system of seven ordinary differential equations for the displacements.

3.5 Finite Element Solution

The system of ordinary differential equations obtained from the equilibrium equations 3.37 is solved in this work using the finite element method. A new finite element has been developed to model the beam problem. This finite element has three nodes and seven degrees of freedom (U, V, W, F, ϕ, α, θ) at each node. The middle node is statically condensed

when solving the problem for displacements, but it is considered when calculating the strain energy release rate, in order to obtain a more accurate solution. The nodal forces and moments for the ith node of the structure are F_x, F_y, F_z, M_z, M_x, W and T.

A quadratic variation of all seven displacements is assumed along the element length. Denoting by X any specific displacement, and by X_i this specific displacement at the ith node, the displacement and deformation within the element are defined as

$$X = a_1 X_1 + a_2 X_2 + a_3 X_3$$
$$X' = b_1 X_1 + b_2 X_2 + b_3 X_3 \tag{3.38}$$

In the last equation, the terms a_1, a_2 and a_2 are interpolation functions in the form of

$$a_1 = 1 - 3\overline{x} + 2\overline{x}^2$$
$$a_2 = \overline{x}(2\overline{x} - 1) \tag{3.39}$$
$$a_3 = 4\overline{x}(1 - 2\overline{x})$$

and b_1, b_2 and b3 are their derivatives with respect to the x direction

$$b_1 = (4\overline{x} - 3)/L$$
$$b_2 = (4\overline{x} - 1)/L \tag{3.40}$$
$$b_3 = 4(1 - 2\overline{x})/L$$

where

$$\overline{x} = x/L$$

In the last equation, L is the element length and x is the coordinate along the beam axis.

By using Eq. 3.38, and the terms a_i and b_i (i=1,2,3) defined in Eqs 3.39 and 3.40, the deformation field (Eq. 3.10) within each finite element as a function of the nodal displacements is expressed in the form of

$$\begin{aligned}(\overline{e}) &= [\overline{a}] \ (q) \\ (\hat{e}) &= [\hat{a}] \ (q)\end{aligned} \tag{3.41}$$

where q is the vector of the displacements

$$\begin{aligned}[q]^T = [&U_1, V_1, W_1, F_1, \phi_1, \alpha_1, \theta_1, \\ &U_2, V_2, W_2, F_2, \phi_2, \alpha_2, \theta_2, \\ &U_3, V_3, W_3, F_3, \phi_3, \alpha_3, \theta_3]\end{aligned} \tag{3.42}$$

and $\bar{a}$ and $\hat{a}$ are two strain-displacement matrices, both with dimension of (5 x 21).

The first strain-displacement matrix, $\bar{a}$, is composed by the following terms:

$$\begin{pmatrix} b_1 & 0 & 0 & 0 & 0 & 0 & 0 & b_2 & 0 & 0 & 0 & 0 & 0 & 0 & b_3 & 0 & 0 & 0 & 0 & 0 & 0 \\ 0 & b_1 & 0 & a_1 & 0 & 0 & 0 & 0 & b_2 & 0 & a_2 & 0 & 0 & 0 & 0 & b_3 & 0 & a_3 & 0 & 0 & 0 \\ 0 & 0 & 0 & 0 & b_1 & 0 & 0 & 0 & 0 & 0 & 0 & b_2 & 0 & 0 & 0 & 0 & 0 & 0 & b_3 & 0 & 0 \\ 0 & 0 & 0 & 0 & 0 & a_1 & -b_1 & 0 & 0 & 0 & 0 & 0 & a_2 & -b_2 & 0 & 0 & 0 & 0 & 0 & a_3 & -b_3 \\ 0 & 0 & b_1 & 0 & a_1 & 0 & 0 & 0 & 0 & b_2 & 0 & a_2 & 0 & 0 & 0 & 0 & b_3 & 0 & a_3 & 0 & 0 \end{pmatrix} \tag{3.43}$$

and the second one, â, of:

$$\begin{pmatrix} 0 & 0 & 0 & b_1 & 0 & 0 & 0 & 0 & 0 & b_2 & 0 & 0 & 0 & 0 & 0 & 0 & b_3 & 0 & 0 & 0 \\ 0 & 0 & 0 & 0 & 0 & 0 & 0 & 0 & 0 & 0 & 0 & 0 & 0 & 0 & 0 & 0 & 0 & 0 & 0 & 0 \\ 0 & 0 & 0 & 0 & 0 & b_1 & 0 & 0 & 0 & 0 & 0 & b_2 & 0 & 0 & 0 & 0 & 0 & 0 & b_3 & 0 \\ 0 & 0 & 0 & 0 & 0 & 0 & 0 & 0 & 0 & 0 & 0 & 0 & 0 & 0 & 0 & 0 & 0 & 0 & 0 & 0 \\ 0 & 0 & 0 & 0 & 0 & a_1 & b_1 & 0 & 0 & 0 & 0 & a_2 & b_2 & 0 & 0 & 0 & 0 & 0 & a_3 & b_3 \end{pmatrix}$$

$$(3.44)$$

Similarly to Eq. 3.10, the total deformation within each element is given by the expression

$$e = \overline{e} + y\hat{e} \tag{3.45}$$

or, after using the strain-displacement matrices, by

$$e = (\overline{a} + y\hat{a}) q \tag{3.46}$$

With

$$a = \overline{a} + y\hat{a} \tag{3.47}$$

the element stiffness matrix is defined as

$$\begin{aligned} K &= \int_0^L \int_{-\frac{b}{2}}^{\frac{b}{2}} a^T D\, a\, dy\, dx \\ &= \int_0^L \int_{-\frac{b}{2}}^{\frac{b}{2}} (\overline{a} + y\hat{a})^T D (\overline{a} + y\hat{a})\, dy\, dx \end{aligned} \tag{3.48}$$

In Eq. 3.48, D is the elasticity matrix for composite materials. The terms in matrix D are the same terms shown in Eq. 3.18. Each term of the matrix D is defined as

$$(A_{ij}, B_{ij}, D_{ij}) = \int_a^b \overline{Q}_{ij} [1, z, z^2] \, dz \qquad (3.49)$$

where a and b are respectively the lowest and highest coordinates in the z direction in the considered element. By defining two element stiffness matrices in the form of

$$\overline{K} = b \int_0^L \overline{a}^T D \, \overline{a} \, dx$$
$$\hat{K} = \frac{b^3}{12} \int_0^L \hat{a}^T D \, \hat{a} \, dx \qquad (3.50)$$

the equation 3.48 is reduced to

$$K = \overline{K} + \hat{K} \qquad (3.51)$$

The elements of the stiffness matrices $\overline{K}$ and $\hat{K}$ are shown in the Appendix. The dimension of the stiffness matrix k are reduced from (21 x 21) to (14 x 14) by using static condensation and the stiffness matrix of each finite element is assembled in a global stiffness matrix, representative of the stiffness of the whole structure.

The final representation of the problem is

$$F = K \, q \qquad (3.52)$$

where K is the total stiffness matrix, and F and q are vectors with the nodal forces and displacements, respectively. In the present work, the equation 3.52 is solved using the Gauss Elimination Method (Bathe, 1982).

3.6 Strain Energy Release Rate

The strain energy release rate is calculated by using the expression for J-integral. A zero volume path is delineated surrounding the crack tip, as shown in Fig. 2.8, and the J-integral expressed in terms of the strain energy per unit length (U) of each element around the crack, as in Eq. 2.55,

$$J = U^{(1)} + U^{(4)} - U^{(2)} - U^{(3)} \qquad (3.53)$$

The strain energy per unit length of the beam (Eq. 3.34) is given by

$$U = \frac{1}{2}\left(b\overline{E}^T D\overline{E} + \frac{b^3}{12} \hat{E}^T D\hat{E} \right) \qquad (3.54)$$

The expression for the strain energy per unit length of the ith element is obtained by substituting Eq. 3.46 in the previous equation.

$$U^{(i)} = \frac{1}{2} q^T\left(b\overline{a}^T D\overline{a} + \frac{b^3}{12} \hat{a}^T D\hat{a} \right) q \qquad (3.55)$$

In Eq. 3.55, the vector q contains the displacements of the nodes of the ith element, including the middle node. The reason for considering the middle node in the calculation of the strain energy is because the static condensation process assumes that no forces or couples are applied to the intermediate node. This assumption is not true for the case where bottom and top offset elements are put together to model the beam.

3.7 Rigid and Gap Elements

The possibility of interference between the crack surfaces in the delaminated region, when the beam is under loading, principally under torsion loading, requires that gap elements or rigid elements be placed in appropriate positions in order to monitor the contact.

Two types of rigid elements are anticipated to be used depending on which side, left or right, of the beam presents the interference phenomenon. Figure 3.3 illustrates the interference situation and the rigid element actions.

In matrix form, the equations of the rigid element placed on the left side can be represented as

$$
\begin{pmatrix}
0 & 0 & 0 & 0 & 1 \\
0 & 0 & 0 & 0 & \dfrac{b}{2} \\
0 & 0 & 0 & 0 & -1 \\
0 & 0 & 0 & 0 & -\dfrac{b}{2} \\
1 & \dfrac{b}{2} & -1 & -\dfrac{b}{2} & 0
\end{pmatrix}
\begin{pmatrix}
W_t \\
\theta_t \\
W_b \\
\theta_b \\
F
\end{pmatrix}
=
\begin{pmatrix}
(F_z)_t \\
T_t \\
(F_z)_b \\
T_b \\
0
\end{pmatrix}
\tag{3.56}
$$

where t and b represent top and bottom elements, respectively, and the force F is shown in Fig. 3.3.

Similarly, the equations of the rigid element placed to on the right side are

$$
\begin{pmatrix}
0 & 0 & 0 & 0 & 1 \\
0 & 0 & 0 & 0 & -\dfrac{b}{2} \\
0 & 0 & 0 & 0 & -1 \\
0 & 0 & 0 & 0 & \dfrac{b}{2} \\
1 & -\dfrac{b}{2} & -1 & \dfrac{b}{2} & 0
\end{pmatrix}
\begin{pmatrix}
W_t \\
\theta_t \\
W_b \\
\theta_b \\
F
\end{pmatrix}
=
\begin{pmatrix}
(F_z)_t \\
T_t \\
(F_z)_b \\
T_b \\
0
\end{pmatrix}
\tag{3.57}
$$

The gap element is placed in the structure to avoid the interference in the delaminated region while the structure is under vertical loading. In matrix form, the constraint equations relative to the gap element are:

$$
\begin{pmatrix}
0 & 0 & 1 \\
0 & 0 & -1 \\
1 & -1 & 0
\end{pmatrix}
\begin{pmatrix}
w_t \\
w_b \\
F
\end{pmatrix}
=
\begin{pmatrix}
(F_z)_t \\
(F_z)_b \\
0
\end{pmatrix}
\tag{3.58}
$$
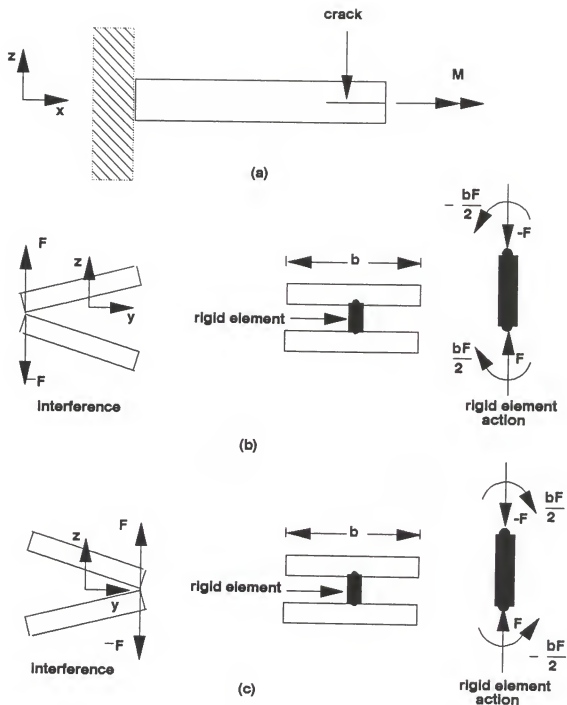
Figure 3.3 Rigid elements: (a) Beam under torsion
(b) Interference on left side (front view)
(c) Interference on right side (front view)

The rigid element and gap element matrices in Eqs. 3.56-3.58 are assembled in the global stiffness matrix using the same procedure adopted to assemble the element stiffness matrices. In Eqs. 3.56-3.58 F_z is the contact force between the interfering elements, T_t or T_b is the couple due to the contact force and F is the force in the rigid or gap element in the z direction.

CHAPTER 4

NUMERICAL RESULTS AND DISCUSSION

4.1 Numerical Results

This chapter presents the numerical results obtained from the finite element described in the previous chapter. Three different tests were performed, and their numerical results compared with those obtained from the beam theory.

The first test of the beam finite element consists of a specially orthotropic cantilever beam subjected to several different end loading conditions. This test is divided into two parts: one in which the beam is modeled using two sublaminates (top and bottom) and the other, where the beam is formed by just the top sublaminate. The purpose of theses tests is to prove the validity of the finite element developed in modeling the beam problem, including the torsion problem.

In the second numerical test, a specially orthotropic delaminated cantilever beam is put under torsion loading. Initially, the delamination is supposed to be in the middle plane of the beam, and the result in terms of the strain energy release rate is compared with the closed-form solution. The delamination is then placed between different layers along the thickness, and a study is performed to understand the

effect of the delamination position on the strain energy release rate.

The last numerical test consists in the simulation of a quasi-static impact test in specially orthotropic and quasi-isotropic simply supported beams. Some experimental observations for this specific tests are available in our Composite Laboratory (Kwon, 1991), and the present numerical study will help interpret the experimental results. Again, the focus was on the effect of the delamination position on the values of the strain energy release rate.

4.2 Material Properties and Stiffness Coefficients

In all the numerical tests performed in the present study, the beam is supposed to be made up of material with the following properties:

Longitudinal Elastic Modulus (E_1): 14.00 GP$_a$

Transverse Elastic Modulus (E_2): 1.00 GP$_a$

Shear Modulus (G_{12}): 0.53 GP$_a$

Poisson's Ratio (v_{12}): 0.30

Poisson's Ratio (v_{23}): 0.55

The above values are typical values for high performance graphite/epoxy unidirectional composites.

Table 4.1 lists the laminate stiffness coefficients for a specially orthotropic beam with thickness equal to 2 mm, and the reference X-Y plane considered to be in the middle

(MIDDLE), on the top (BOTTOM) or on the bottom (TOP) surfaces of the beam.

4.3 Cantilever Beam

The dimensions of the beam are 0.2 m x 0.02 m x 0.002 m (length x width x thickness), and the beam is subjected to a set of six different end loading conditions, as shown in Fig. 4.1 and Fig. 4.3.

4.3.1 Model with two sublaminates

Initially, the beam subjected to the forces shown in Fig. 4.1 is modeled by using two connected sublaminates (top and bottom), as shown in Fig. 4.2. Table 4.2 presents the numerical and beam theory solutions, in terms of the displacements at the tip of the beam for each of the loading conditions.

The expressions for beam theory results can be found in Timoshenko (1970), Reissman and Pawlik (1980) and Sankar (1991), or can be derived from the beam equations presented in Sankar (1991). In the following expressions the superscripts t and b stands for top and bottom, respectively.

4.3.1.1 Beam under Force 1 (F_1)

In this case, we have just the U displacement. All other displacements are zero.

Table 4.1 Stiffness coefficients

STIFFNESS COEFFICIENTS	POSITION OF THE X AXIS		
	TOP	BOTTOM	MIDDLE
A_{11}	0.2818173E8	0.2818173E8	0.2818173E8
A_{16}	0.0	0.0	0.0
A_{66}	0.1066621E7	0.1066621E7	0.1066621E7
B_{11}	0.2818229E5	-0.2818229E5	0.0
B_{16}	0.0	0.0	0.0
B_{66}	0.1066643E4	-0.1066643E4	0.0
D_{11}	0.3757714E2	0.3757714E2	0.9394285E1
D_{16}	0.0	0.0	0.0
D_{66}	0.1422219E1	0.1422219E1	0.3555547
$K^2 A_{55}$	0.8888511E6	0.8888511E6	0.8888511E6
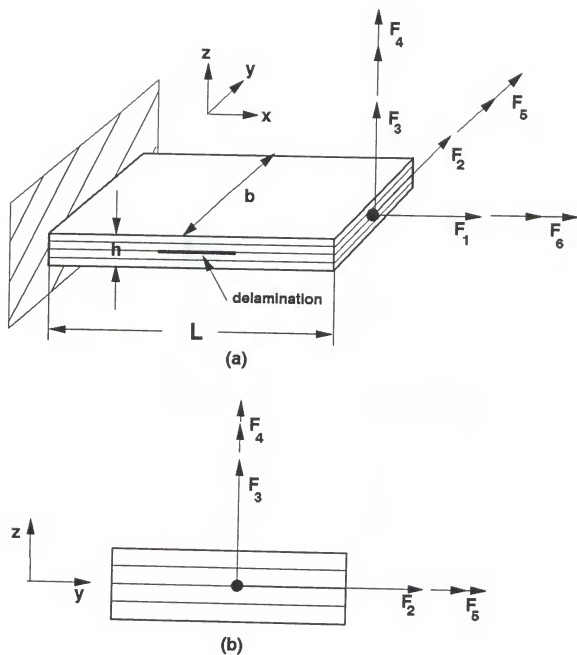
Figure 4.1 Loading conditions at middle plane
(a) Perspective view   (b) Front view
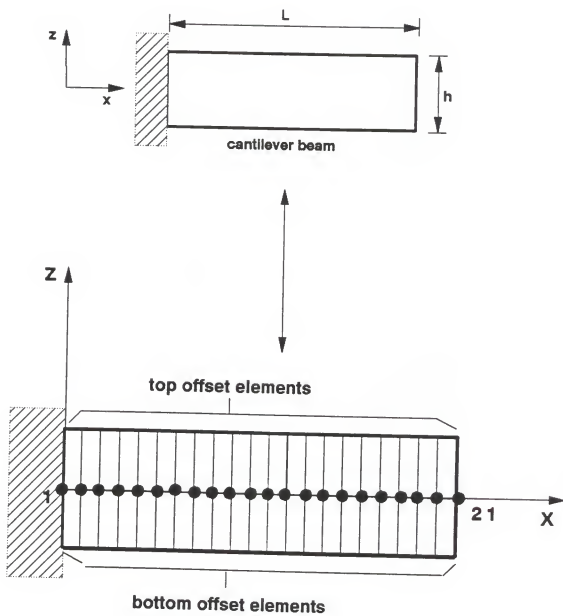
Figure 4.2 Model with 42 elements

Table 4.2 Displacements for model with 42 elements

FORCES		DISPLACEMENTS AT THE TIP OF THE BEAM						
		U (m)	V (m)	W (m)	F (rad)	ϕ (rad)	σ (rad)	θ (rad)
1	FEM	3.55E-7	0.0	0.0	0.0	0.0	0.0	0.0
	BEAM	3.55E-7	0.0	0.0	0.0	0.0	0.0	0.0
2	FEM	0.0	1.51E-4	0.0	1.06E-3	0.0	0.0	0.0
	BEAM	0.0	1.64E-4	0.0	1.06E-3	0.0	0.0	0.0
3	FEM	0.0	0.0	0.0142	0.0	0.1064	0.0	0.0
	BEAM	0.0	0.0	0.0142	0.0	0.1064	0.0	0.0
4	FEM	0.0	-1.06E-3	0.0	0.0106	0.0	0.0	0.0
	BEAM	0.0	-1.07E-3	0.0	0.0107	0.0	0.0	0.0
5	FEM	0.0	0.0	-0.1064	0.0	1.0645	0.0	0.0
	BEAM	0.0	0.0	-0.1064	0.0	1.0645	0.0	0.0
6	FEM	0.0	0.0	0.0	0.0	0.0	-34.7343	6.6082
	BEAM	0.0	0.0	0.0	0.0	0.0	-34.7343	7.0312

$$U = F_1 \frac{L}{b(A^t{}_{11} + A^b{}_{11})} \tag{4.1}$$

4.3.1.2 Beam under Force 2 (F_2)

Under Force 2 the beam has the displacements V and F. The remaining five displacements are zero.

$$V = F_2\left(\frac{4L^3}{b^3(A^t{}_{11} + A^b{}_{11})} + \frac{2L}{b(A^t{}_{55} + A^b{}_{55})}\right) \tag{4.2}$$

$$F = -F_2 \frac{6L^2}{b^3(A^t{}_{11} + A^b{}_{11})} \tag{4.3}$$

4.3.1.3 Beam under Force 3 (F_3)

From this case results the displacements W and ϕ.

$$W = F_3\left(\frac{L^3}{3b(D^t{}_{11} + D^b{}_{11})} + \frac{2L}{b(A^t{}_{55} + A^b{}_{55})}\right) \tag{4.4}$$

$$\phi = F_3 \frac{1}{2} \frac{L^2}{b(D^t{}_{11} + D^b{}_{11})} \tag{4.5}$$

4.3.1.4 Beam under Force 4 (F^4)

The displacements under Force 4 are V and F. The remaining displacements are zero.

$$V = -F_4 \frac{6L^2}{b^3(A^t{}_{11} + A^b{}_{11})} \tag{4.6}$$

$$F = F_4 \frac{12L}{b^3 (A^t_{11} + A^b_{11})} \tag{4.7}$$

4.3.1.5 Beam under Force 5 (F_5)

Under this loading condition the displacements are W and ϕ, and all others are zero.

$$W = -F_5 \frac{1}{2} \frac{L^2}{b (D^t_{11} + D^b_{11})} \tag{4.8}$$

$$\phi = F_5 \frac{L}{b (D^t_{11} + D^b_{11})} \tag{4.9}$$

4.3.1.6 Beam under Force 6 (F_6)

The displacements under Force 6 are θ and α. The displacement θ is given by the expression (Sankar, 1991b)

$$\theta = F_6 \frac{L}{4b (D^t_{66} + D^b_{66})} \left(1 + \frac{D^t_{66} + D^b_{66}}{D^t_{55} + D^b_{55}} \right) \tag{4.10}$$

where

$$D^t_{55} + D^b_{55} = \frac{b^2}{12} k^2 (A^t_{55} + A^b_{55}) \tag{4.11}$$

and

$$k^2 = \frac{5}{6} \tag{4.12}$$

while the displacement α is defined as

$$\alpha = C_1 \cosh(x) + C_2 \sinh(x) - C_3 \frac{12}{b^3 \lambda^2 (D^t_{11} + D^b_{11})} \tag{4.13}$$

where

$$C_1 = F_6 \frac{12}{b^3 \lambda^2 (D^t_{11} + D^b_{11})} \frac{D^{**}_{55}}{D^{**}_{66}} \tag{4.14}$$

$$C_2 = -C_1 \lambda \sinh(x) \tag{4.15}$$

and

$$C_3 = \frac{D^{**}_{55}}{D^{**}_{66}}$$

In Eqs. 4.13-4.16,

$$X = L \sqrt{\frac{48 (D^t_{66} + D^b_{66})(D^t_{55} + D^b_{55})}{b^2 (D^t_{11} + D^b_{11}) D^{**}_{66}}} \tag{4.17}$$

$$\lambda^2 = \frac{12 D^{**}_{66}}{b^2 (D^t_{11} + D^b_{11})} \tag{4.18}$$

$$D^{**}_{55} = \frac{1}{12} b^2 \kappa^2 (A^{t}_{55} + A^{b}_{55}) - \frac{1}{4} (D^{t}_{66} + D^{b}_{66}) \tag{4.19}$$

$$D^{**}_{66} = \frac{1}{12} b^2 \kappa^2 (A^{t}_{55} + A^{b}_{55}) + \frac{1}{4} (D^{t}_{66} + D^{b}_{66}) \tag{4.20}$$

4.3.2 Model with top sublaminate

In a second test, the beam is modeled using top offset elements only (Fig. 4.3). The beam is subjected to the set of loading conditions displayed in Fig. 4.3. Table 4.3 shows the numerical and closed solutions for this test. The sources for the beam theory solutions presented in Table 4.3 are the same used before: Timoshenko (1970), Reismann and Pawlik (1980) and Sankar (1991b). Some expressions are derived from the beam equations.

4.3.2.1 Beam under Force 1 (F₁)

The tip displacements under F_1 are U, W and ϕ. The remaining displacements are zero.

$$U = F_1 \frac{L}{b \cdot A^{t}_{11}} \tag{4.21}$$

$$W = \frac{F_1}{2} \frac{(\frac{h}{2}) L^2}{b(\frac{D^{t}_{11}}{4})} \tag{4.22}$$
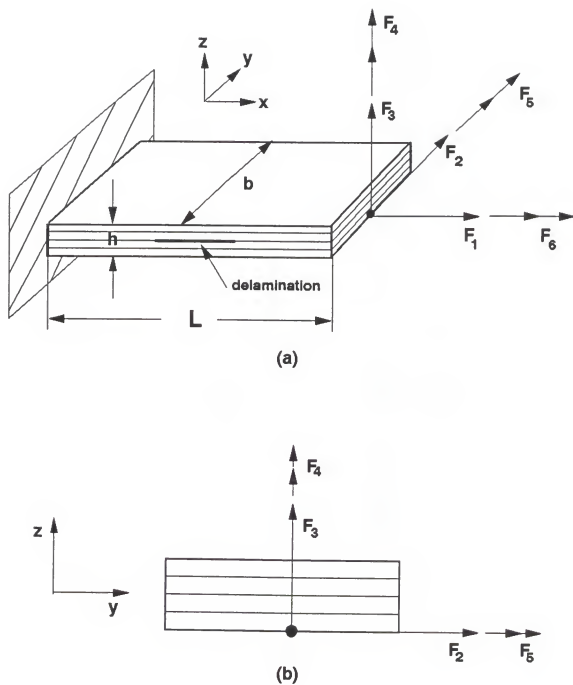
Figure 4.3 Loading conditions at the bottom plane
(a) Perspective view (b) Front view
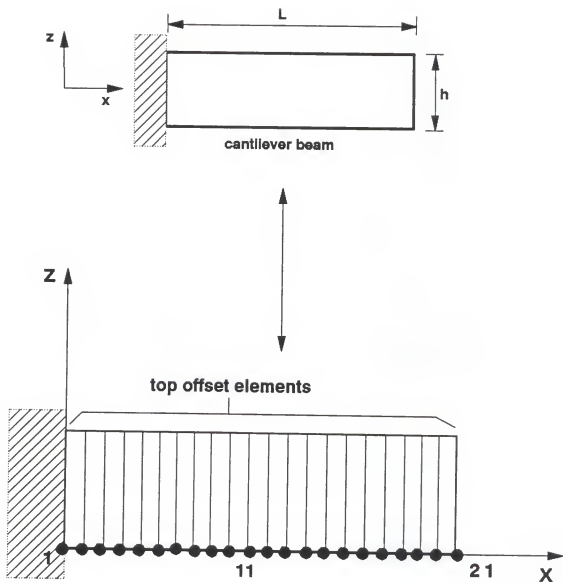
Figure 4.4 Model with 21 elements

Table 4.3 Displacements for model with 21 elements

FORCES		DISPLACEMENTS AT THE TIP OF THE BEAM						
		U (m)	V (m)	W (m)	F (rad)	ϕ (rad)	σ (rad)	θ (rad)
1	FEM	1.42E-6	0.0	1.06E-4	0.0	-1.06E-3	0.0	0.0
	BEAM	1.42E-6	0.0	1.06E-4	0.0	-1.06E-3	0.0	0.0
2	FEM	0.0	1.58E-4	0.0	1.03E-3	0.0	-0.0347	6.66E-3
	BEAM	0.0	1.71E-4	0.0	1.06E-3	0.0	-0.0347	7.03E-3
3	FEM	1.06E-4	0.0	0.0142	0.0	0.1064	0.0	0.0
	BEAM	1.06E-4	0.0	0.0142	0.0	0.1064	0.0	0.0
4	FEM	0.0	-1.03E-3	0.0	0.0130	0.0	-2.3776	0.0347
	BEAM	0.0	-1.07E-3	0.0	0.0107	0.0	-0.516	0.1068
5	FEM	0.0	0.0	-0.1064	0.0	1.0644	0.0	0.0
	BEAM	0.0	0.0	-0.1064	0.0	1.0644	0.0	0.0
6	FEM	0.0	6.61E-3	0.0	0.0347	0.0	-34.7343	6.6082
	BEAM	0.0	7.03E-3	0.0	0.0351	0.0	-34.7343	7.0312

$$\phi = -F_1 \frac{(\frac{h}{2}) \, L}{b \, (\frac{D^t_{11}}{4})} \tag{4.23}$$

4.3.2.2 Beam under Force 2 (F_2)

In the case of a cantilever beam under F_2 the tip displacements are V, F, θ and α.

The displacement V can be represented as

$$V = V_1 + V_2 \tag{4.24}$$

where

$$V_1 = (F2) \left(\frac{4L^3}{b^3 A^t_{11}} + \frac{2L}{bA^t_{55}} \right) \tag{4.25}$$

and

$$V_2 \qquad h \tag{4.26}$$

The displacement θ is necessary to calculate V_2 and is defined as

$$\theta = F_2 \frac{\frac{h}{2} \, L}{b \, D^t_{66}} \left(1 + \frac{(\frac{D^t_{66}}{4})}{D^t_{55}} \right) \tag{4.27}$$

where the term D^t_{55} is defined as

$$D^t_{55} = \frac{1}{12} b^2 k^2 A^t_{55} \tag{4.28}$$

The displacement F is given by

$$F = -F_2 \frac{6 L^2}{b^3 A^t_{11}} \tag{4.29}$$

Finally, the expression for the displacement α is

$$\alpha = C_1 \cosh(X) + C_2 \sinh(X) - C_3 \frac{48}{b^3 \lambda^2 D^t_{11}} \tag{4.30}$$

where

$$C_1 = F_6 \frac{48}{b^3 \lambda^2 D^t_{11}} \frac{D^{**}_{55}}{D^{**}_{66}} \tag{4.31}$$

$$C_2 = -C_1 \lambda \sinh(X) \tag{4.32}$$

and

$$C_3 = \frac{D^{**}_{55}}{D^{**}_{66}} \tag{4.33}$$

In Eqs. 4.30-4.33,

$$X = L \sqrt{\frac{48 \, D^t_{66} D^t_{55}}{b^2 D^t_{11} \, D^{**}_{66}}} \tag{4.34}$$

$$\lambda^2 = \left(\frac{12 D^{**}_{66}}{b^2 D_{11}} \right) \tag{4.35}$$

$$D^{**}_{55} = \frac{1}{12} b^2 \kappa^2 A^t_{55} - \frac{1}{4} D^t_{66} \tag{4.36}$$

$$D^{**}_{66} = \frac{1}{12} b^2 \kappa^2 A^t_{55} + \frac{1}{4} D^t_{66} \qquad (4.37)$$

and the term D^t_{55} is defined as

$$D^t_{55} = \frac{1}{12} b^2 k^2 A^t_{55} \qquad (4.38)$$

4.3.2.3 Beam under Force 3 (F_3)

Under force F_3, the beam presents three displacements: U, W and ϕ. They are defined as

$$W = F_3 \left(\frac{4L^3}{3 bD^t_{11}} + \frac{2L}{bA^t_{55}} \right) \qquad (4.39)$$

and

$$U = \phi \frac{h}{2} \qquad (4.41)$$

4.3.2.4 Beam under Force 4 (F_4)

The displacements in this case are V, F, α and θ. The remaining displacements are zero. This case can be considered as the result of the addition of two different loadings, I and II, as shown in Figure 4.5.

Figure 4.5 Beam under loading F_4
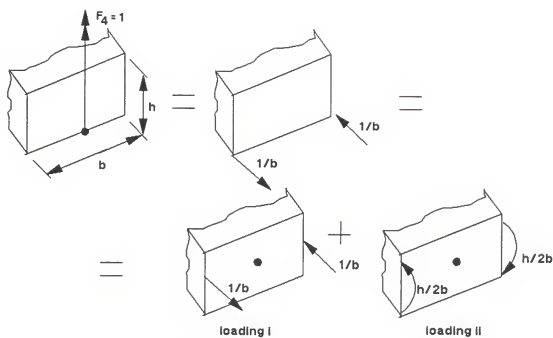
The displacements for the Loading I were calculated as explained in the Section 4.3.1.4. From Loading II results the displacements α and θ, which are calculated using the following expressions (Sankar, 1991b):

$$\alpha - C_8 \sinh(\lambda L) \tag{4.42}$$

where C_8 is a constant defined as

$$C_8 - \frac{12\hat{M}_x}{b^3 D_{11}} \frac{1}{\lambda \cosh(\lambda L)} \tag{4.43}$$

where the constant λ is calculated using Eq. 4.18.

From the definition given in Eq. 3.20, we have that

$$
\begin{aligned}
\hat{M}_x &= \int_{-b/2}^{\frac{b}{2}} M_x dy \\
&= -2\frac{b}{2}\frac{h}{2b} \\
&= -\frac{h}{2}
\end{aligned}
\tag{4.44}
$$

The rotation θ is given by

$$\theta' = -C_3 \alpha$$

where the constant C_3 is defined in Eq. 4.16.

Considering the boundary condition $\theta(0)=0$, we have

$$\theta(x) = -C_3 \alpha L$$

Loading I does not produce α or θ displacements. Hence, the α and θ displacements calculated using the previous equations are the result for the total loading.

The displacement F is given by Eq. 4.7 and the displacement V is obtained using the expression

$$V = V_1 + \theta\frac{h}{2} \tag{4.47}$$

where V_1 is given by Eq. 4.6.

4.3.2.5 Beam under Force 5 (F_5)

Under force F_5 the displacements are U, W and ϕ. The remaining displacements are zero.

where the displacement ϕ is given by

$$U = -\frac{h}{2}\phi \qquad (4.48)$$

$$\phi = F_5 \frac{4\ L}{b\ D^t_{11}} \qquad (4.49)$$

The displacement W is defined as

$$W = -F_5 \frac{2\ L^2}{b\ D^t_{11}} \qquad (4.50)$$

4.3.2.6 Beam under Force 6 (F_6)

In this case the displacements are V, F, α and θ.

$$V = \frac{h}{2}\ \theta \qquad (4.51)$$

where the rotation θ is calculated using the expression

$$\theta = F_6 \frac{L}{b\ D^t_{66}}\left(1\ +\ \frac{D^t_{66}}{4\ D^t_{55}}\right) \qquad (4.52)$$

The rotation F is defined as

$$F = \tan^{-1}(\frac{V}{L}) \qquad (4.53)$$

and the warping function α can be obtained using Eqs. 4.30–4.37.

4.3.3 Comments on the finite element solution

Tables 4.2 and 4.3 show a very good agreement between the present finite element solutions and the analytical results derived from beam theory. This agreement can also be seen in

Figures 4.6 and 4.7, in which is shown the angle of twist along the beam length for two cantilever beams with different lengths. The beams are under a unit torque, and in both cases they were modeled by ten finite elements. From these figures, we can see that in the region close to the support the agreement is not good, and probably it will require use of larger number of finite elements near the fixed support.

The beam theory solution for this case (Sankar, 1991b) incorporates the edge effect, represented by the third term in brackets on the right hand side of Eq. 4.52, and is given by the following expression

$$\theta(x) = F_6 \frac{x}{4\, b D_{66}} \theta(L) \tag{4.54}$$

where $\theta(x)$ and $\theta(L)$ are the angle of twist at a distance x from the fixed support and at the tip of the beam, respectively.

The tip rotation of a beam, $\theta(L)$, is given by

$$\theta_{(L)} = 1 + \frac{D_{66}}{D_{55}} - \frac{\left(1 - \dfrac{D_{66}}{D_{55}}\right)^2}{\left(1 + \dfrac{D_{66}}{D_{55}}\right)} \frac{\tanh\,(\lambda b)}{\lambda L} \tag{4.55}$$

In Eqs. 4.54 and 4.55 we have that

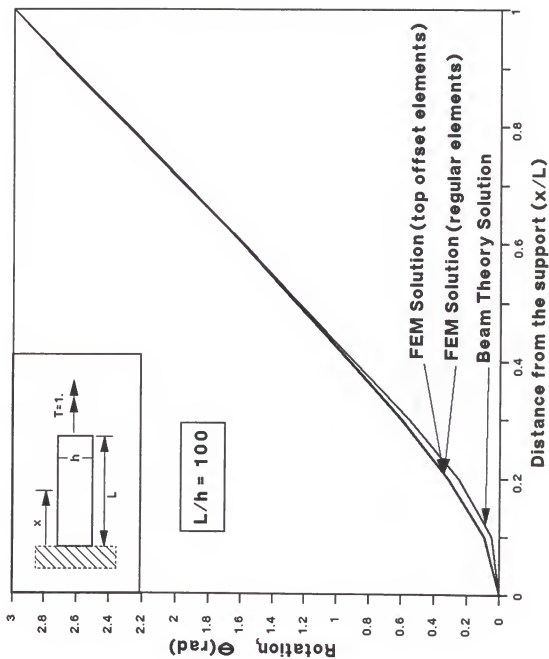$$\lambda = \sqrt{\frac{48\, D_{66} D_{55}}{b^2 D_{11} \overline{D}_{66}}} \tag{4.56}$$

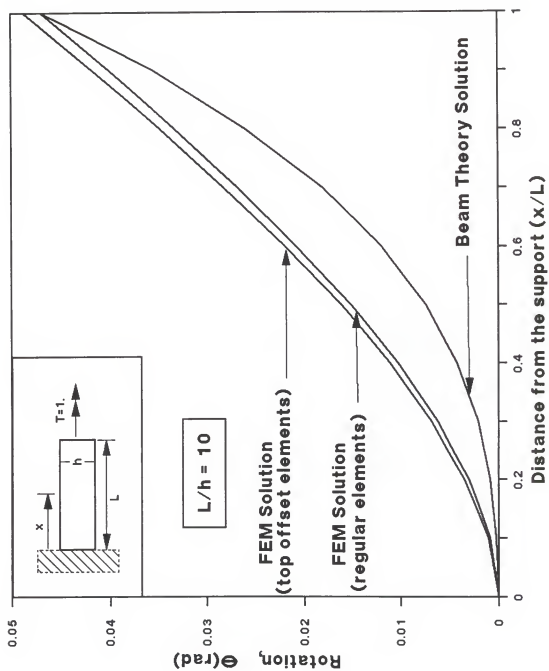Figure 4.6 Angle of twist along the length (L/h=100)

Figure 4.7 Angle of twist along the length (L/h=10)

and

$$D_{55} - \left(\frac{b^2}{12}\right)\kappa^2 A_{55} \qquad (4.57)$$

$$\overline{D}_{66} - D_{66} + \left(\frac{b^2}{12}\right)k^2 A_{55}$$

where k^2 is a shear correction factor, considered equal to 5/6 in the present work.

4.4 Delaminated Cantilever Beam under Torsion

In the present application, the beam is assumed to have a delamination of length 20 mm. The dimensions of the beam are 0.60 m x 0.02 m x 0.002 m. The length of the beam and of the delamination were enlarged if compared with the beam used in the previous examples. The reason was to avoid the edge effect, so as to be able to model the problem using fewer finite elements.

A unit torque is applied at the free end of the beam, and the strain energy released is computed. The numerical result is then compared with the closed-form solution obtained using the beam theory (Sankar, 1991b). Figure 4.8, (a) and (b), shows the beam under torsion and the model used to obtain the closed-form solution, while Fig. 4.9 illustrates the finite element model used to solve the problem. In this model, middle-plane beam finite elements are used in the uncracked regions, behind and beyond the delamination, (regions 1 and 3), while top and bottom offset elements are used in the cracked portion of the beam (region 2). Later, the
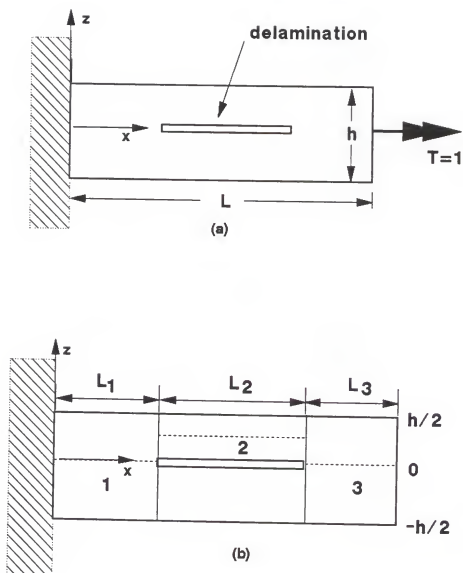
Figure 4.8 Delaminated beam

(a) Under torsion   (b) Separated by parts
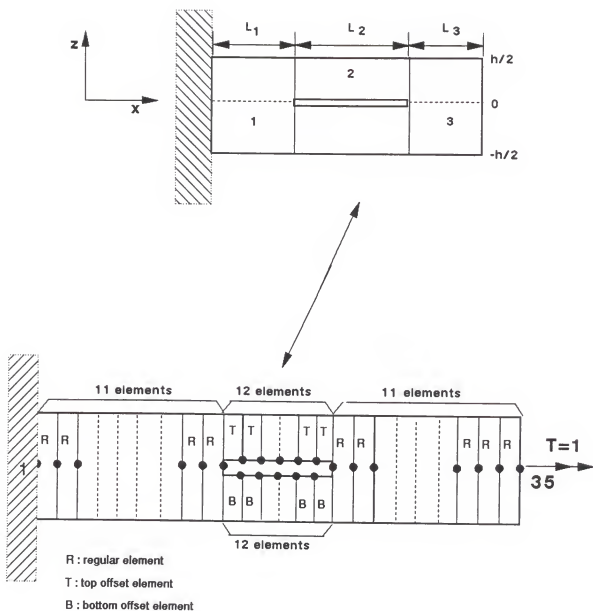
Figure 4.9 Finite element model

delamination will be assumed in different positions along the thickness of the beam, the strain energy release rate will be computed for each of these positions.

4.4.1 Delamination at the middle-plane of the beam

The finite element model used to solve this case has forty-six nodes and forty-six elements, as shown in Fig. 4.9. There are twenty-two regular finite elements and twenty-four offset elements (twelve top elements and twelve bottom elements).

Referring to Fig. 4.8(b) and to the strain energy release rate (G) definition (Hellan, 1984) we have

$$G = \frac{\partial U}{\partial A} = \frac{1}{b} \frac{\partial U}{\partial L_2} \qquad (4.58)$$

where U is the strain energy of the beam and A is the crack area. In the present case, the area of the crack is formed by a rectangle with dimensions equal to b and L_2.

The strain energy of the beam (U) is defined as

$$U = \frac{1}{2} T \theta(L) \qquad (4.59)$$

where T is the torque and $\theta(L)$ is the rotation θ at the tip of the beam.

The rotation at the tip of the beam is calculated by adding the rotations in the three parts of the beam shown in Figure 4.7, and is defined by

$$\theta_L - \theta_1 + \theta_2 + \theta_3 \qquad (4.60)$$

where the subscripts stand for the regions in the beam (Fig. 4.8(b)).

By definition,

$$A_{ij} - \int_{h_i}^{h_s} C_{ij}\, dz$$
$$D_{ij} - \int_{h_i}^{h_s} C_{ij} z^2\, dz \qquad (4.61)$$

where the integration limits h_s and h_i stand respectively for the superior and inferior limits of the beam in the z direction.

The parts 1 and 3 of the beam have the same integration limits, h/2 and -h/2, while for part 2 they are h/4 and -h/4. Considering these integration limits and solving Eq. 4.61, we obtain the following relations among the stiffness coefficients of the three parts of the beam:

$$(A_{ij})_1 - (A_{ij})_3 - 2\,(A_{ij})_2$$
$$(D_{ij})_1 - (D_{ij})_3 - 8\,(D_{ij})_2 \qquad (4.62)$$

By using Eqs. 4.54, 4.55 and 4.60, and neglecting the edge effect, the rotation at the tip of the beam is now expressed as

$$\theta(L) - \frac{T(L_1 + L_3)}{4\,b}\left(\frac{1}{D_{66}} + \frac{1}{D_{55}}\right) + \frac{TL_2}{b}\left(\frac{1}{D_{66}} + \frac{1}{4\,D_{55}}\right) \qquad (4.63)$$

Referring to Fig. 4.8(b), we have that

$$L_1 + L_3 = L - L_2 \qquad (4.64)$$

Substituting Eq. 4.64 in Eq. 4.63 gives

$$\theta(L) = \frac{T(L-L_2)}{4b}\left(\frac{1}{D_{66}} + \frac{1}{D_{55}}\right) + \frac{TL_2}{b}\left(\frac{1}{D_{66}} + \frac{1}{4D_{55}}\right) \qquad (4.65)$$

Using Eq.4.59 we obtain the strain energy of the beam (U) as

$$U = \frac{T^2(L-L_2)}{8b}\left(\frac{1}{D_{66}} + \frac{1}{D_{55}}\right) + \frac{T^2 L_2}{b}\left(\frac{1}{2D_{66}} + \frac{1}{8D_{55}}\right) \qquad (4.66)$$

Considering Eq. 4.58, we obtain the following expression for strain energy release rate (G)

$$G = \frac{T^2}{b^2}\left(-\frac{1}{8}\left(\frac{1}{D_{66}} + \frac{1}{D_{55}}\right) + \left(\frac{1}{2D_{66}} + \frac{1}{8D_{55}}\right)\right) \qquad (4.67)$$

or, after simplifying the last equation,

$$G = \frac{3}{8}\frac{T^2}{b^2 D_{66}} \qquad (4.68)$$

Substituting in the last equation the values of

$$T = 1 \ Nm$$
$$b = 0.02m$$
$$D_{66} = 0.3556 \ \frac{N}{m^2}m^3$$

we obtain for the strain energy release rate the value of 2,636.0 J/m^2, while the numerical result for the present case is 2,545.5 J/m^2. The relative difference between numerical and closed-form solutions is 3.45%.

4.4.2 Delamination position varying along the thickness

In this example, the delamination was assumed to be in different positions along the thickness of the beam. The procedure adopted here is similar to that used to calculate the strain energy release rate with the delamination placed in the middle plane, except for the integration limits when calculating the stiffness coefficients A_{ij}, B_{ij} and D_{ij}.

Figure 4.10 illustrates the adopted model for the case of delamination placed between layers close to the top. Table 4.4 presents the obtained results for different positions of the delamination along the thickness of the beam. These results are also depicted in Figure 4.11. From Figure 4.11, we can conclude that the possibility of crack propagation will be increased as the crack position approaches the middle plane of the beam. As the crack plane approaches the top or bottom faces of the beam, the strain energy release rate becomes negative. This could be due to errors in the energy calculations, and can be avoided by having shorter elements near the crack tip. This problem should be subjected to further investigations.
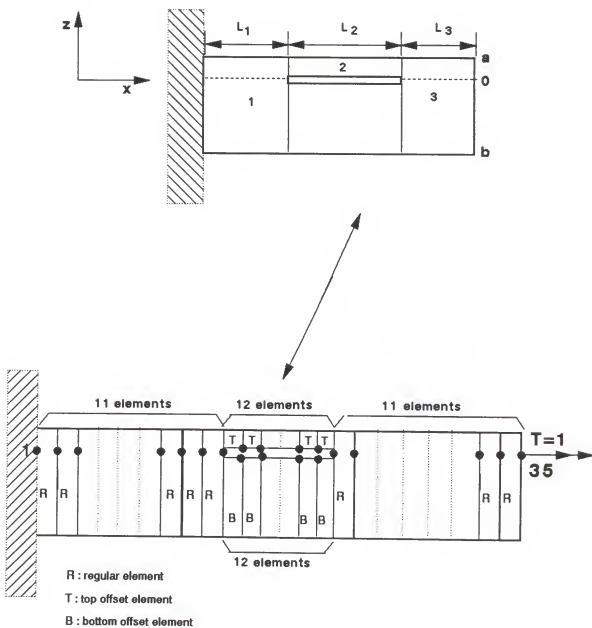
Figure 4.10 Delamination close to the top plane

Table 4.4 Strain energy release rate (G) for cantilever

beam

POSITION	G (J/m^2)
between layers 1 and 2	-17.5
between layers 2 and 3	173.2
between layers 3 and 4	653.8
between layers 4 and 5	1,409.9
between layers 5 and 6	2,195.1
between layers 6 and 7	2,545.5
between layers 7 and 8	2,195.5
between layers 8 and 9	1,409.9
between layers 9 and 10	653.8
between layers 10 and 11	173.2
between layers 11 and 12	-17.5
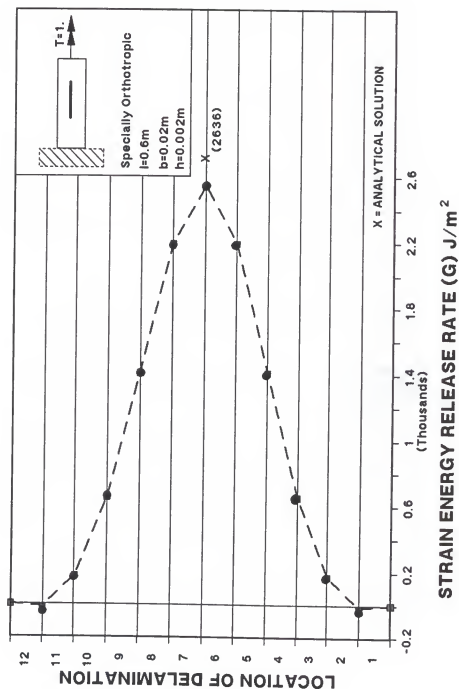
Figure 4.11 Strain energy release rate for cantilever beam

4.5 Simply Supported Beam under Transverse Force

In this section we consider the problem of transverse loading on a simply supported beam (Figure 4.12).

The dimensions of the beam, the length of the delamination, the material and the finite element model are the same as in the preceding example. A force equal to 100 N is applied to the center of the beam. The finite element model is shown in Figure 4.12.

Two classes of laminates were analyzed, a specially orthotropic laminate and a [0/45/-45/90]s laminate. The delamination was assumed in different positions along the laminate thickness, and the results for each class of laminate are listed in Table 4.5 and shown in Figure 4.13.

Similarly to the cantilever beam case, from the present results we can conclude that the possibility of crack propagation will be increased as the crack position approaches the middle-plane of the beam. This phenomenon is less pronounced in the specially orthotropic beam than in the other beam. Another conclusion is that for a given transverse force, the possibility of crack propagation is more in the [0/45/-45/90]s laminate.

These results have an important application in understanding the propagation of delamination damage in composite laminates due to low-velocity impact as well as quasi-static indentation types of loading (Kwon, 1991).
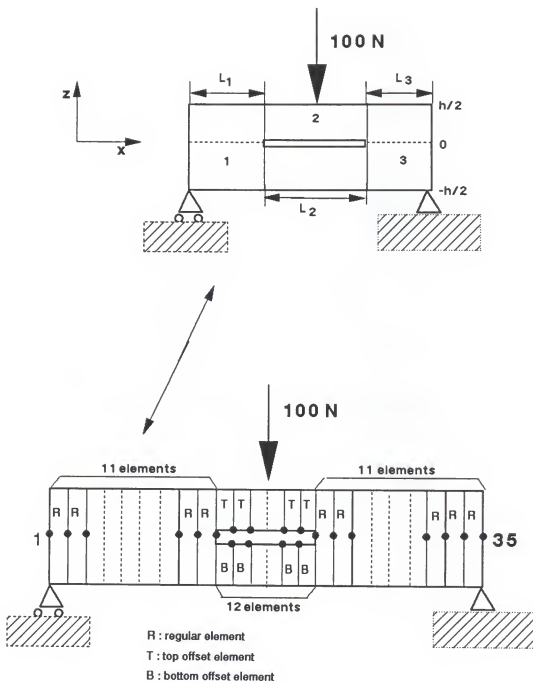
Figure 4.12 Simply supported beam

Table 4.5 Strain energy release rate (G) for simply

        supported beam

POSITION	G (J/m^2)	
	Specially orthotropic	[0/45/-45/90]s
between layers 1 and 2	406.9	1,945.0
between layers 2 and 3	1,071.0	5,858.0
between layers 3 and 4	1,971.0	10,070.0
between layers 4 and 5	2,495.0	11,390.0
between layers 5 and 6	1,971.0	10,070.0
between layers 6 and 7	1,071.0	5,858.0
between layers 7 and 8	406.9	1,945.0
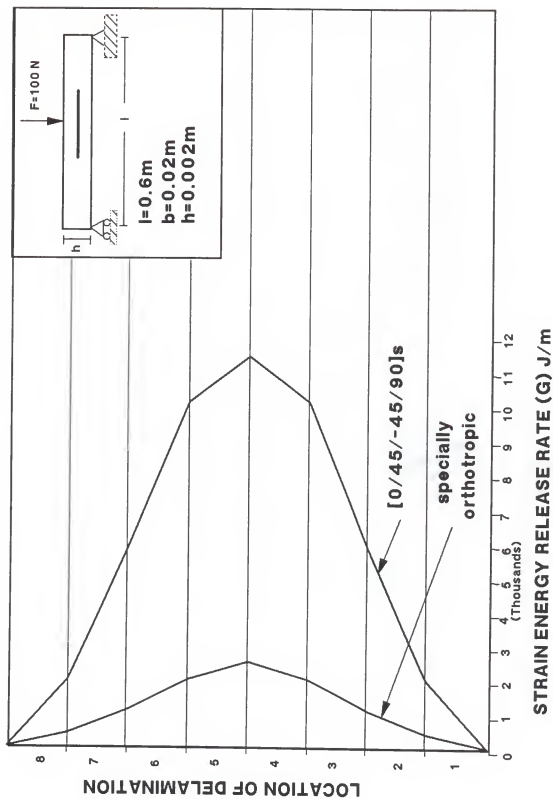
Figure 4.13 Strain energy release rate for simply supported beam

CHAPTER 5

SUMMARY AND FUTURE RESEARCH

5.1 Summary

The present investigation was restricted to delaminations in laminated beams. Finite elements were developed to model specific cases of delaminations, and the numerical results were compared with results from other methods and approaches.

A laminated shear deformable beam finite element with nodes offset to either top or bottom has been developed to analyze free edge delaminations. These offset elements were used to model the sublaminates above and below the delamination plane. A rigid element was used to connect the nodes at the crack tip, and the forces and moments transmitted by this rigid element are part of the finite element solution of the problem. The strain energy release rate was calculated using expressions derived from the J-integral, the crack tip force method and crack closure method. These expressions are in terms of displacements and forces in the elements surrounding the crack-tip, which are part of the finite element solution. The present method considers the effect caused by the thermal stresses induced in the composite layers during the curing process.

There are some advantages in using the present method. The finite element method has great flexibility in modeling any kind of geometry, loading and boundary conditions. This makes it easier to model common specimens used in laboratory experiments and compare results. In modeling the cracked region of the beam by using offset node elements, one can avoid renumbering the nodes as the crack propagates. It tremendously saves computer storage and time involved in redefining nodes.

The delamination in anisotropic beams was analyzed using a new beam finite element to model the problem. The formulation of this new beam finite element is based on a beam theory for laminated beams in which the equilibrium equations are assumed to be satisfied in an average sense over the width of the beam. A new set of force and moment resultants for the beam were introduced from this assumption. Two problems of practical interest were solved using this method. One of them was the problem of a specially orthotropic delaminated cantilever beam under torsion loading, and the other was the case of specially orthotropic and quasi-orthotropic simply supported beams under transverse loading. In both problems the delamination was assumed to be in different positions along the thickness of the beam, and the strain energy release rate for each position was computed. The strain energy release rate was found to have the maximum value in the middle plane of the beam, for both the cantilever beam under torsion and the

simply supported beam under transverse force. Practically, this indicates that the probability of crack propagation becomes higher as the position of the delamination approaches the middle plane of the beam.

5.2 Future research

The present method has almost all its results validated by comparison with other methods and approaches. The method needs to be applied in an extensive body of experimental tests.

The extension of this method to the study of buckling in laminated composite beams will add an important possibility in composite structural mechanics.

One suggestion that naturally arises from this study is to extend the presently developed method to three-dimensional fracture problems, to compute strain energy release rate in delaminated plates. The study of plates with multiple delaminations can be an important sequel to this research.

The final suggestion is the extension of this method to dynamic problems, which will bring significant benefits to both research in impact dynamics and design of composite materials. Then, this work will have achieved an important goal in the process of simulation of delaminations and crack propagation.

APPENDIX

STIFFNESS MATRIX

The subroutine STIFF is used to form the stiffness matrix K of the beam finite element used in modeling anisotropic laminated beams. The matrix K results from the addition of two matrices, $\overline{K}$ and $\hat{K}$.

$$K = \overline{K} + \hat{K}$$

Figure A illustrates the formation process of matrix K and it is important for understanding the subroutine steps. The final result is the matrix C, with dimension of 14 x 14.

The input to the subroutine STIFF are:

B: width of the beam

SV: vector with the stiffness terms for top, bottom and regular elements.

XLE: element length

IX1: integer that defines the element type: 1 for top element, 2 for bottom element and 3 for regular element.

The output of the subroutine STIFF are:

CC: matrix (7,7) (see Fig. A.1)

CA: matrix (7,14)(see Fig. A.1)

C: matrix (14,14), representative of the stiffness of the beam finite element.
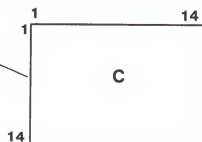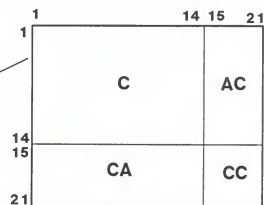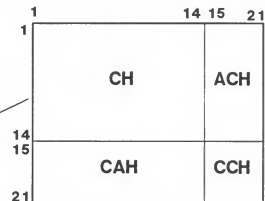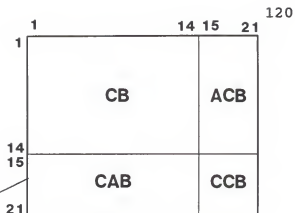
Figure A Stiffness matrix K

```fortran
      SUBROUTINE STIFF(B,SV,XLE,IX1,CC,CA,C)
      IMPLICIT DOUBLE PRECISION(A-H,O-Z)
      DIMENSION SV(30),CB(14,14),CH(14,14),C(14,14)
      DIMENSION C1(14,7),C2(14,14),CC(7,7),AC(14,7),CA(7,14)
      DIMENSION ACB(14,7),ACH(14,7),CAB(7,14),CAH(7,14)
      DIMENSION CCB(7,7),CCH(7,7)
      II=10*(IX1-1)
      A11=SV(II+1)
      A16=SV(II+2)
      A66=SV(II+3)
      B11=SV(II+4)
      B16=SV(II+5)
      B66=SV(II+6)
      D11=SV(II+7)
      D16=SV(II+8)
      D66=SV(II+9)
      A55=SV(II+10)
      DO 1 I=1,14
      DO 1 J=1,14
      C(I,J)=0.0
1     CONTINUE
      DO 5 I=1,14
      DO 5 J=1,14
      CB(I,J)=0.0
      CH(I,J)=0.0
      C2(I,J)=0.0
5     CONTINUE
      DO 10 I=1,7
      DO 10 J=1,7
      CC(I,J)=0.0
      CCB(I,J)=0.0
      CCH(I,J)=0.0
10    CONTINUE
      DO 15 I=1,14
      DO 15 J=1,7
      AC(I,J)=0.0
      CA(J,I)=0.0
      ACB(I,J)=0.0
      CAB(J,I)=0.0
      ACH(I,J)=0.0
      CAH(J,I)=0.0
      C1(I,J)=0.0
15    CONTINUE
C.....'BAR' MATRICES...................
C.....CB(14,14).......................
      CB(1,1)=A11*(70./XLE)
      CB(1,2)=A16*(70./XLE)
      CB(1,4)=A16*(-15.)
      CB(1,5)=B11*(70./XLE)
      CB(1,6)=B16*(-15.)
      CB(1,7)=B16*(-70./XLE)
      CB(1,8)=A11*10./XLE
```

```
CB(1,9)=A16*10./XLE
CB(1,11)=A16*5.
CB(1,12)=B11*10./XLE
CB(1,13)=B16*5.
CB(1,14)=B16*(-10./XLE)
CB(2,2)=A66*(70./XLE)
CB(2,4)=A66*(-15.)
CB(2,5)=-CB(1,7)
CB(2,6)=B66*(-15)
CB(2,7)=B66*(-70./XLE)
CB(2,8)=CB(1,9)
CB(2,9)=A66*10./XLE
CB(2,11)=A66*5.
CB(2,12)=-CB(1,14)
CB(2,13)=B66*5.
CB(2,14)=B66*(-10./XLE)
CB(3,3)=A55*(70./XLE)
CB(3,5)=A55*(-15.)
CB(3,10)=A55*10./XLE
CB(3,12)=A55*5.
CB(4,4)=A66*4.*XLE
CB(4,5)=CB(1,6)
CB(4,6)=B66*4.*XLE
CB(4,7)=-CB(2,6)
CB(4,8)=-CB(1,11)
CB(4,9)=-CB(2,11)
CB(4,11)=A66*(-XLE)
CB(4,12)=-CB(1,13)
CB(4,13)=B66*(-XLE)
CB(4,14)=CB(2,13)
CB(5,6)=D16*(-15)
CB(5,5)=D11*(70./XLE)+A55*4.*XLE
CB(5,7)=D16*(-70./XLE)
CB(5,8)=CB(1,12)
CB(5,9)=-CB(1,14)
CB(5,10)=-CB(3,12)
CB(5,11)=CB(1,13)
CB(5,12)=D11*10./XLE+A55*(-XLE)
CB(5,13)=D16*5.
CB(5,14)=D16*(-10./XLE)
CB(6,6)=D66*4.*XLE
CB(6,7)=D66*15
CB(6,8)=-CB(1,13)
CB(6,9)=-CB(2,13)
CB(6,11)=CB(4,13)
CB(6,12)=-CB(5,13)
CB(6,13)=D66*(-XLE)
CB(6,14)=D66*5.
CB(7,7)=D66*70./XLE
CB(7,8)=CB(1,14)
CB(7,9)=CB(2,14)
CB(7,11)=-CB(2,13)
```

```
      CB(7,12)=CB(5,14)
      CB(7,13)=-CB(6,14)
      CB(7,14)=D66*10./XLE
      CB(8,8)=A11*70./XLE
      CB(8,9)=A16*70./XLE
      CB(8,11)=A16*15.
      CB(8,12)=B11*70./XLE
      CB(8,13)=B16*15.
      CB(8,14)=CB(1,7)
      CB(9,9)=CB(2,2)
      CB(9,11)=-CB(2,4)
      CB(9,12)=-CB(1,7)
      CB(9,13)=-CB(2,6)
      CB(9,14)=CB(2,7)
      CB(10,10)=CB(3,3)
      CB(10,12)=-CB(3,5)
      CB(11,11)=CB(4,4)
      CB(11,12)=-CB(1,6)
      CB(11,13)=CB(4,6)
      CB(11,14)=CB(2,6)
      CB(12,12)=D11*70./XLE+A55*4.*XLE
      CB(12,13)=D16*15.
      CB(12,14)=CB(5,7)
      CB(13,13)=CB(6,6)
      CB(13,14)=-CB(6,7)
      CB(14,14)=CB(7,7)
      DO 20 I=1,14
      DO 20 J=I,14
      CB(J,I)=CB(I,J)
20    CONTINUE
      DO 18 I=1,14
      DO 18 J=1,14
      CB(I,J)=CB(I,J)*B/30.
18    CONTINUE
C.....MATRIX ACB(14,7).............
      ACB(1,1)=A11*(-80./XLE)
      ACB(1,2)=A16*(-80./XLE)
      ACB(1,4)=A16*(-20.)
      ACB(1,5)=B11*(-80./XLE)
      ACB(1,6)=B16*(-20.)
      ACB(1,7)=B16*(80./XLE)
      ACB(2,1)=ACB(1,2)
      ACB(2,2)=A66*(-80./XLE)
      ACB(2,4)=A66*(-20.)
      ACB(2,5)=-ACB(1,7)
      ACB(2,6)=B66*(-20.)
      ACB(2,7)=B66*(80./XLE)
      ACB(3,3)=A55*(-80./XLE)
      ACB(3,5)=A55*(-20.)
      ACB(4,1)=A16*20.
```

```
ACB(4,2)=A66*20.
ACB(4,4)=A66*2.*XLE
ACB(4,5)=B16*20.
ACB(4,6)=B66*2.*XLE
ACB(4,7)=B66*(-20.)
ACB(5,1)=ACB(1,5)
ACB(5,2)=-ACB(1,7)
ACB(5,3)=A55*20.
ACB(5,4)=-20.*B16
ACB(5,5)=D11*(-80./XLE)+A55*2.*XLE
ACB(5,6)=D16*(-20.)
ACB(5,7)=D16*80./XLE
ACB(6,1)=ACB(4,5)
ACB(6,2)=-ACB(4,7)
ACB(6,4)=ACB(4,6)
ACB(6,5)=D16*20.
ACB(6,6)=D66*2.*XLE
ACB(6,7)=D66*(-20.)
ACB(7,1)=ACB(1,7)
ACB(7,2)=ACB(2,7)
ACB(7,4)=-ACB(2,6)
ACB(7,5)=ACB(5,7)
ACB(7,6)=D66*(20.)
ACB(7,7)=D66*(-80./XLE)
ACB(8,1)=ACB(1,1)
ACB(8,2)=ACB(1,2)
ACB(8,4)=ACB(4,1)
ACB(8,5)=ACB(1,5)
ACB(8,6)=ACB(4,5)
ACB(8,7)=ACB(1,7)
ACB(9,1)=ACB(1,2)
ACB(9,2)=ACB(2,2)
ACB(9,4)=ACB(4,2)
ACB(9,5)=-ACB(1,7)
ACB(9,6)=-ACB(4,7)
ACB(9,7)=ACB(2,7)
ACB(10,3)=ACB(3,3)
ACB(10,5)=A55*20.
ACB(11,1)=-ACB(4,1)
ACB(11,2)=-ACB(4,2)
ACB(11,4)=ACB(4,4)
ACB(11,5)=-ACB(4,5)
ACB(11,6)=ACB(4,6)
ACB(11,7)=20.*B66
ACB(12,1)=ACB(1,5)
ACB(12,2)=-ACB(1,7)
ACB(12,3)=-ACB(5,3)
ACB(12,4)=20.*B16
ACB(12,5)=D11*(-80./XLE)+A55*2.*XLE
ACB(12,6)=ACB(6,5)
ACB(12,7)=ACB(5,7)
```

```
      ACB(13,1)=-ACB(4,5)
      ACB(13,2)=ACB(4,7)
      ACB(13,4)=ACB(4,6)
      ACB(13,5)=-ACB(6,5)
      ACB(13,6)=D66*2.*XLE
      ACB(13,7)=D66*(20.)
      ACB(14,1)=ACB(1,7)
      ACB(14,2)=ACB(2,7)
      ACB(14,4)=ACB(4,7)
      ACB(14,5)=ACB(5,7)
      ACB(14,6)=ACB(6,7)
      ACB(14,7)=ACB(7,7)
      DO 24 I=1,14
      DO 24 J=1,7
      ACB(I,J)=ACB(I,J)*B/30.
24    CONTINUE
C.....CAB(7,14)................
      DO 25 I=1,14
      DO 25 J=1,7
      CAB(J,I)=ACB(I,J)
25    CONTINUE
C.....CC(7,7)..................
      CCB(1,1)=A11*160./XLE
      CCB(1,2)=A16*160./XLE
      CCB(1,5)=B11*160./XLE
      CCB(1,7)=-B16*160./XLE
      CCB(2,2)=A66*160./XLE
      CCB(2,5)=-CCB(1,7)
      CCB(2,7)=B66*(-160./XLE)
      CCB(3,3)=A55*160./XLE
      CCB(4,4)=A66*16.*XLE
      CCB(4,6)=B66*16.*XLE
      CCB(5,5)=D11*160./XLE+A55*16.*XLE
      CCB(5,7)=D16*(-160./XLE)
      CCB(6,6)=D66*16.*XLE
      CCB(7,7)=D66*160./XLE
      DO 28 I=1,7
      DO 28 J=I,7
      CCB(I,J)=CCB(I,J)*B/30.
28    CONTINUE
      DO 26 I=1,7
      DO 26 J=I,7
      CCB(J,I)=CCB(I,J)
26    CONTINUE
C.....'HAT' MATRICES ...........
C.....CH(14,14)................
      BB=B**3/12.
      CH(4,4)=A11*70./XLE
      CH(4,6)=B11*70./XLE
      CH(4,11)=A11*10./XLE
      CH(4,13)=B11*10./XLE
```

```
      CH(6,6)=(D11*70./XLE)+(A55*4.*XLE)
      CH(6,7)=A55*(-15.)
      CH(6,11)=CH(4,13)
      CH(6,13)=(D11*10./XLE)+A55*(-XLE)
      CH(6,14)=A55*(-5.)
      CH(7,7)=A55*70./XLE
      CH(7,13)=-CH(6,14)
      CH(7,14)=A55*10./XLE
      CH(11,11)=CH(4,4)
      CH(11,13)=CH(4,6)
      CH(13,13)=CH(6,6)
      CH(13,14)=-CH(6,7)
      CH(14,14)=CH(7,7)
      DO 55 I=1,14
      DO 55 J=I,14
      CH(J,I)=CH(I,J)
55    CONTINUE
      DO 60 I=1,14
      DO 60 J=1,14
      CH(I,J)=CH(I,J)*BB/30.
60    CONTINUE
C.....ACH(14,7)...............
      ACH(4,4)=BB*(A11*(-80./XLE))/30.
      ACH(4,6)=BB*(B11*(-80./XLE))/30.
      ACH(6,4)=BB*(B11*(-80./XLE))/30.
      ACH(6,6)=BB*(D11*(-80.)/XLE+A55*2.*XLE)/30.
      ACH(6,7)=BB*(A55*20.)/30.
      ACH(7,6)=BB*(A55*(-20.))/30.
      ACH(7,7)=BB*(A55*(-80./XLE))/30.
      ACH(11,4)=BB*(A11*(-80./XLE))/30.
      ACH(11,6)=BB*(B11*(-80./XLE))/30.
      ACH(13,4)=BB*(B11*(-80./XLE))/30.
      ACH(13,6)=BB*(D11*(-80.)/XLE+A55*2.*XLE)/30.
      ACH(13,7)=-BB*(A55*20.)/30.
      ACH(14,6)=BB*(A55*20.)/30.
      ACH(14,7)=BB*(A55*(-80./XLE))/30.
C.....CAH(7,14)...............
      DO 65 I=1,14
      DO 65 J=1,7
      CAH(J,I)=ACH(I,J)
65    CONTINUE
C.....CCH(7,7)...............
      CCH(4,4)=BB*(A11*160./XLE)/30.
      CCH(4,6)=BB*(B11*160./XLE)/30.
      CCH(6,6)=BB*((D11*160./XLE)+(A55*16.*XLE))/30.
      CCH(7,7)=BB*(A55*160./XLE)/30.
```

```
      DO 70 I=1,7
      DO 70 J=I,7
      CCH(J,I)=CCH(I,J)
70    CONTINUE
C.....ADDING THE 'BAR' AND 'HAT' MATRICES.....
      DO 30 I=1,14
      DO 30 J=1,14
      C(I,J)=CB(I,J)+CH(I,J)
30    CONTINUE
      DO 32 I=1,14
      DO 32 J=1,7
      AC(I,J)=ACB(I,J)+ACH(I,J)
      CA(J,I)=CAB(J,I)+CAH(J,I)
32    CONTINUE
      DO 34 I=1,7
      DO 34 J=1,7
      CC(I,J)=CCB(I,J)+CCH(I,J)
34    CONTINUE
C.....STATIC CONDENSATION....................
      CALL INVDET(CC,7)
      CALL MATMUL(AC,CC,C1,14,7,7)
      CALL MATMUL(C1,CA,C2,14,7,14)
      DO 40 I=1,14
      DO 40 J=1,14
      C(I,J)=C(I,J)-C2(I,J)
40    CONTINUE
      CALL INVDET(CC,7)
      RETURN
      END
```

REFERENCES

Agarwal, B. D. and Broutman, L. J., <u>Analysis and Performance of Fiber Composites</u>, John Wiley & Sons, New York, NY, 1980.

Armanios, E. A. and Badir, A., <u>Hygrothermal Influence on the Edge Delamiantion in Composites</u>, Technomic Publishing Company, Lancaster, Pennsylvania, 1989

Bathe, K. J., <u>Finite Element Procedures in Engineering Analysis</u>, Prentice-Hall, Englewood Cliffs, New Jersey, 1982.

Chan, W. S. and Ochoa, O. O., "An Integrated Finite Element Model of Edge-Delamination Analysis for Laminates Due to Tension, Bending, and Torsion Loads," Proceedings of AIAA/ASME/ASCE/AHS/ASC 28th SDM conference, Monterey, California, 1987, pp. 27-35.

Hellan, K., <u>Introduction to Fracture Mechanics</u>, McGraw-Hill, New York, New York, 1984.

Hu, S., Sankar, B. V. and Sun, C. T., "A Finite Element Study of Dynamic Delamination Growth in Composite Laminates," Proceedings of AIAA/ASME/ASCE/AHS/ASC 30th SDM conference, Mobile, Alabama, 1989, pp. 1250-1255.

Kwon, Y.S.,"Indentation-Flexure Damage in Graphite/Epoxy Laminates," Master Thesis, University of Florida, Gainesville, Florida, 1991

Pagano, N. J., "On the Calculation of Interlaminar Normal Stress in Composite Laminate," J. Composite Materials, Vol. 8, 1974, p. 65.

Pagano, N. J., <u>Interlaminar Response of Composite Materials</u>, Elsevier Science Publishing Company, New York, New York, 1989

Raju, I. S., "Q3DG - A Computer Program for Strain Energy Release Rate for Delamination Growth in Composite Laminates," NASA CR - 178205 (1986), 103 p.

Reismann, H. and Pawlik, P. S., _Elasticity Theory and Applications_, John Wiley & Sons, New York, 1980.

Sankar, B. V., "A Finite Element for Modeling Delaminations in Composite Beams," Computers & Structures, Vol. 38, N^0 2, pp. 239-246, 1991a.

Sankar, B. V., "A Beam Theory for Laminated Composites and Application to Torsion Problems," AeMES TR-91-1-01, 1991b.

Sankar, B. V. and Pinheiro, M. A., "An Offset Beam Finite Element for Fracture Analysis of Delaminations," Proceedings of AIAA/ASME/ASCE/AHS/ASC 31th SDM conference, Long Beach, California, 1990, pp. 1227-1233.

Tauchert, T. R., _Energy Principles in Structural Mechanics_, McGraw-Hill, New York, 1974.

Timoshenko, S. P. and Goodier, J. N., _Theory of Elasticity_, Mc Graw-Hill, New York, 1970.

Usman, M. and Gandhi, M. V., "The Effect of Moisture and temperature on the Vibrational Characteristcs of Composite Materials," Proceedings of the American Society for Composites, 4th conference, 1989, pp. 555-579.

Whitney, J. M., "Stress Analysis of a Mode I Edge Delamination Specimen for Composite Materials," AIAA Journal, Vol. 24, N^0 7, 1986, pp.1163-1168.

Whitney, J. M., _Structural Analysis of Laminated Anisotropic Plates_, Technomic Publishing Company, Lancaster, Pennsylvania, 1987.

BIOGRAPHICAL SKETCH

Marco Antonio Santos Pinheiro was born on August 3, 1947, in Rio de Janeiro, Brazil. He is married to Fernanda Elizabeth Pinto Pinheiro and has two children, Simone, 20, and Luis Marco, 17.

He joined the Brazilian Army in 1966, entering the Agulhas Negras Military Academy as a cadet. He graduated in 1969 and was commissioned as lieutenant in the Army Ordnance Corps.

In 1975 he entered the Military Institute of Engineering, located in Rio de Janeiro, and received the bachelor's degree in mechanical engineering in 1977. As a result of the grade points average achieved, he received the "Henry Ford Award," given by the Ford Brazil Company. This award consists of a specialization in automotive engineering, with visits to automotive plants and research centers during a period of six months.

After being technical director and leader of a military plant in the industrial city of Sao Paulo for two years, working and participating in the process of development and fabrication of armored cars and other heavy equipments for the Army, he was invited to be an instructor at the Military

Institute of Engineering, in the city of Rio de Janeiro. He joined the faculty at this Institute in 1980 and taught undergraduate level courses in the field of automotive engineering until 1989. In the same period, he taught undergraduate courses at a private engineering school, the University Gama Filho, also in the city of Rio de Janeiro. These courses were in the area of mechanical materials and designs.

He started his master's degree program in 1985 at the same Institute, defending his thesis on "Dynamic Analysis of Armored Cars" in October of 1987. After receiving his master's degree in mechanical engineering, he was selected by the Brazilian Army to pursue doctoral studies at the University of Florida, in the Department of Aerospace Engineering, Mechanics and Engineering Science.